2019

FTN Signaling-Aided Space-Time Multi-Mode Index Modulation Systems With a GMP-Based Receiver

Shaoang Li

Nan Wu

Qiaolin Shi

Qinghua Guo
University of Wollongong, qguo@uow.edu.au

FTN Signaling-Aided Space-Time Multi-Mode Index Modulation Systems With a GMP-Based Receiver

Abstract

In this paper, we propose a faster-than-Nyquist (FTN) signaling-aided space-time multi-mode index modulation (IM) scheme with a low-complexity Gaussian message passing (GMP) based receiver. The advantages of spatial domain IM, time-domain IM relying on multiple modes and FTN signaling are explored. Specifically, multi-mode IM is employed in time domain by activating all time slots, hence the spectral efficiency is improved substantially compared to its single-mode counterpart. Meanwhile, the transmission rate is further increased by utilizing FTN signaling. At the receiver, based on the state-space model of IM symbols, a two-layer Forney style factor graph (FG) representation for the system is constructed to exploit the truncated inter-symbol interference structure imposed by FTN. Belief propagation is invoked to update the messages over the FG. The discrete messages from the channel decoder are properly approximated to be Gaussian for reducing the complexity of joint detection of multidimensional index modulated symbols. Moreover, the extrinsic information from the equalizer is derived with a concise representation. A low-complexity log-likelihood ratio calculation method is further proposed, where the search space is significantly reduced using a Gaussian mixture model. Simulation results demonstrate that the proposed scheme outperforms the existing schemes in terms of bit error rate given the same spectral efficiency. The outstanding performance and low complexity of the proposed GMP-based receiver are also verified by comparisons with existing methods.

Keywords

signaling-aided, space-time, multi-mode, index, ftn, modulation, receiver, systems, gmp-based

Disciplines

Engineering | Science and Technology Studies

Publication Details

S. Li, N. Wu, Q. Shi & Q. Guo, "FTN Signaling-Aided Space-Time Multi-Mode Index Modulation Systems With a GMP-Based Receiver," IEEE Access, vol. 7, pp. 162898-162912, 2019.

IEEE Access
Multidisciplinary | Rapid Review | Open Access Journal

Received October 17, 2019, accepted November 4, 2019, date of publication November 7, 2019, date of current version November 19, 2019.

Digital Object Identifier 10.1109/ACCESS.2019.2952259

FTN Signaling-Aided Space-Time Multi-Mode Index Modulation Systems With a GMP-Based Receiver

SHAOANG LI[1], NAN WU[1], (Member, IEEE), QIAOLIN SHI[1], (Student Member, IEEE), AND QINGHUA GUO[2,3], (Senior Member, IEEE)

[1]School of Information and Electronics, Beijing Institute of Technology, Beijing 100081, China
[2]School of Electrical, Computer and Telecommunications Engineering, University of Wollongong, Wollongong, NSW 2522, Australia
[3]School of Engineering, The University of Western Australia, Perth, WA 6009, Australia

Corresponding author: Nan Wu (wunan@bit.edu.cn)

This work was supported in part by the National Science Foundation of China under Grant 61971041, Grant 61571041, and Grant 61471037.

ABSTRACT In this paper, we propose a faster-than-Nyquist (FTN) signaling-aided space-time multi-mode index modulation (IM) scheme with a low-complexity Gaussian message passing (GMP) based receiver. The advantages of spatial domain IM, time-domain IM relying on multiple modes and FTN signaling are explored. Specifically, multi-mode IM is employed in time domain by activating all time slots, hence the spectral efficiency is improved substantially compared to its single-mode counterpart. Meanwhile, the transmission rate is further increased by utilizing FTN signaling. At the receiver, based on the state-space model of IM symbols, a two-layer Forney style factor graph (FG) representation for the system is constructed to exploit the truncated inter-symbol interference structure imposed by FTN. Belief propagation is invoked to update the messages over the FG. The discrete messages from the channel decoder are properly approximated to be Gaussian for reducing the complexity of joint detection of multidimensional index modulated symbols. Moreover, the extrinsic information from the equalizer is derived with a concise representation. A low-complexity log-likelihood ratio calculation method is further proposed, where the search space is significantly reduced using a Gaussian mixture model. Simulation results demonstrate that the proposed scheme outperforms the existing schemes in terms of bit error rate given the same spectral efficiency. The outstanding performance and low complexity of the proposed GMP-based receiver are also verified by comparisons with existing methods.

INDEX TERMS Index modulation, faster-than-Nyquist signaling, factor graph, belief propagation, Gaussian mixture model, state-space model.

I. INTRODUCTION

The recent concept of index modulation (IM) has attracted numerous attention, since this novel digital modulation scheme is highly spectrum- and energy-efficient [1]–[3]. Being different from conventional modulation schemes in which the information bits are conveyed by constellation alphabets, IM scheme utilizes the indices of building blocks (e.g., antennas, subcarriers, time slots, *etc.*) to convey additional information bits. As a result, the additional information bits, which are usually known as *index bits*, can be transmitted through the patterns of indexed building blocks without extra energy consumption, leading to significant increase in spectral and energy efficiency [1].

IM scheme can be employed in spatial domain, time domain, frequency domain, *etc*. When implemented in spatial domain, the IM scheme, which is also referred to as spatial modulation (SM) [4]–[6], activates a fraction of transmit antennas at a time. By converting classical information bits to index bits conveyed by the activation pattern of antennas, the inter-channel interference (ICI) can be significantly reduced. The frequency-domain IM scheme with orthogonal frequency division multiplexing (OFDM), also known as OFDM-IM [7], [8], utilizes the indices of OFDM subcarriers to transmit index bits, enhancing the spectral and energy efficiency of traditional OFDM which cannot meet the

The associate editor coordinating the review of this manuscript and approving it for publication was Wasiu Oyewole Popoola.

increasing requirements in the fifth generation networks [9]. By performing the index modulation on time slots of symbol blocks, the time-domain IM can be implemented [10], [11]. The aforementioned IM schemes with inactivated building blocks are known as single-mode index modulation (SIM). Due to the 'null signal' during transmission, the spectral efficiency of SIM is restricted. To overcome the limitation of SIM, multi-mode index modulation (MIM) is introduced in [12]–[14]. In [13], a dual-mode time-domain IM system is proposed. By conveying the index bits through the combination pattern of a dual-mode signal constellation, the transmission rate is significantly increased. A multi-mode OFDM-IM (OFDM-MIM) scheme is proposed in [14]. However, similar to the conventional OFDM scheme, OFDM-MIM suffers high peak-to-average power ratio (PAPR).

On the other hand, IM can be combined in multiple domains, leading to multidimensional IM. Exploiting the advantages of IM scheme in multiple dimensions, the system performance of multi-mode IM scheme can be enhanced compared with its single domain counterpart. In [15], a multi-mode IM scheme is developed, where IM matrices obtaining patterns of constellation modes employed in both time slots and OFDM subcarriers are introduced. The generalized multiple-mode OFDM-IM scheme proposed in [16] allows the utilization of signal constellations with different sizes. Comprehensive design guidelines further guarantee the optimal asymptotic BER performance. Additionally, coordinate interleave and linear constellation precoding techniques are applied in [17] to attain high diversity gain and high spectral efficiency. Another utilization of IM in both time domain and spatial domain leads to the space-time shift keying scheme. A fraction of dispersion matrices is selected for data transmission, whose indices carry additional index bits, with flexible trade-off between diversity gain and multiplexing gain [18], [19]. In [20] and [21], the index modulation scheme with multidimensional building blocks is introduced, while both of them, though, employ SIM in time domain, whose transmission rate, as mentioned above, is limited.

In IM scheme, since the index bits correspond to the pattern of a certain amount of building blocks, integrated IM subframe containing all the building blocks should be jointly detected at the receiver. Moreover, in the channel-encoded IM system, the index bits have to be taken into account when calculating the extrinsic log-likelihood ratio (LLR), which is significantly different from the traditional systems. The maximum-likelihood (ML) detector is often employed in IM-aided systems [1]. However, the computational complexity of ML detector increases substantially when the size of IM subframe becomes large. Consequently, it is of great significance to devise low-complexity detectors for channel-encoded IM systems, especially for the multidimensional IM as the size of IM subframe is further expanded. In [10], a time-domain single carrier (SC) IM system without channel coding is proposed with frequency domain equalization (FDE) and symbol-by-symbol ML exhaustive search. In [22], an OFDM-IM system with channel encoding is proposed, in which the LLR is calculated based on a reduced-complexity ML detector where the soft information calculation is complicated [1]. In [23], a time-domain turbo equalizer is devised based on the soft minimum mean squared error (MMSE) equalization [24]–[26]. The SC-FDE detector is extended to multiple-input-multiple-output (MIMO) SM system in [6] using a block-wise circular channel matrix representation. However, the linear FDE may suffer from noise enhancement over deep frequency-selective fading channels [27]. In [21], a two-step detector is proposed for multi-dimensional IM system without iterative turbo equalization, whose computational complexity increases substantially as the length of transmission blocks grows.

Among several methods to further improve the transmission rate of IM scheme, the faster-than-Nyquist (FTN) signaling, which is proposed by Mazo in 1970s [28] and has been rediscovered recently [29], [30], is able to increase the transmission rate without extra bandwidth utilization. More specifically, through packing the symbol period by a ratio less than 1, the signal can be transmitted faster without decreasing the minimum Euclidean distance (MED) of signals given that the packing ratio is above a certain threshold, i.e. the *Mazo limit*. Only a few studies focused on the FTN signaling-aided IM scheme. A time-domain SIM system with FTN signaling is proposed in [11], which demonstrates that the MED is further increased when the packing factor is above the Mazo limit due to the sparse structure of SIM scheme. In [13], the FTN signaling is also amalgamated with the dual-mode IM scheme, which leads to an additional increase in the transmission rate. However, both of the above works employ the IM system without channel coding. To the best of our knowledge, low-complexity turbo equalization has not been investigated for FTN signaling-aided IM systems.

Recently, inspired by the factor graph (FG) models [31], iterative receivers based on message passing algorithms are devised in several researches [32]–[34]. The probabilistic relation between variables can be visualized utilizing the graphical representation of system model, and flexible message passing algorithms can be derived with the structure of the FG.

In this paper, we propose an FTN-aided space-time domain multi-mode IM system, namely *STMIM-FTN*, with a GMP-based receiver. The major contributions of this paper are summarized as follows.

- We propose an FTN signaling-aided STMIM system with channel coding. Different from the existing works in [11], [20] and [21], we consider a more efficient multi-mode IM scheme in time domain. Meanwhile, the multidimensional IM scheme is able to exploit not only the advantages of time-domain IM scheme, but also the superiority of SM. FTN signaling is employed to further increase the spectral efficiency of the proposed scheme.
- At the receiver, to reduce the computational complexity owing to the equalization of FTN signaling and the detection of multidimensional IM scheme, we devise

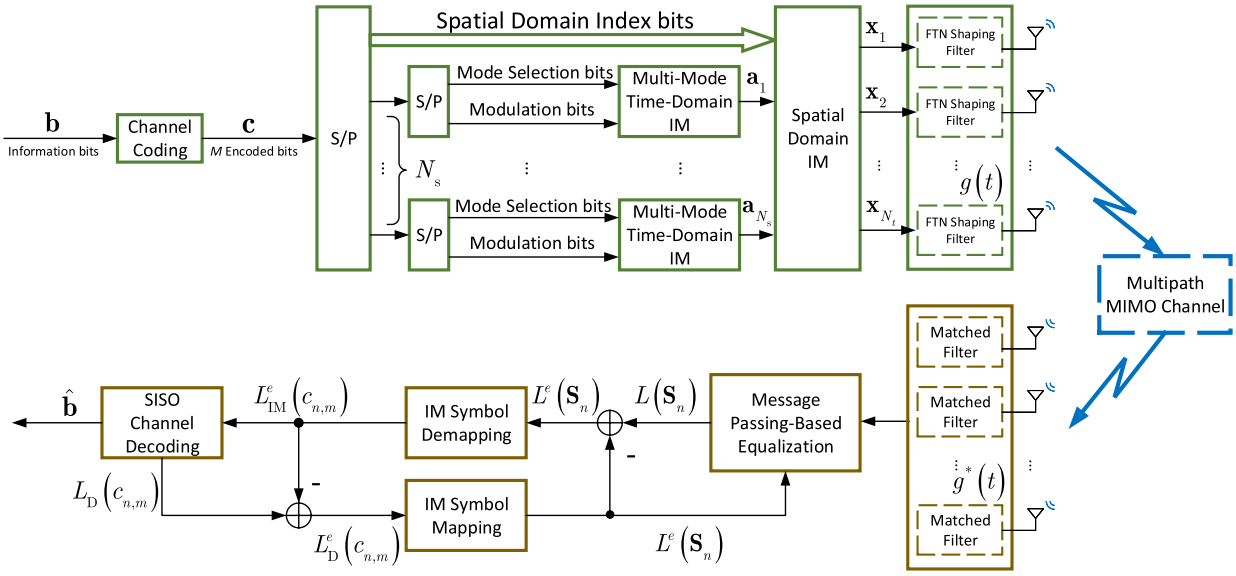

FIGURE 1. The block diagram of the STMIM-FTN transmitter and receiver.

an FG-based low-complexity message passing algorithm. Different from [35] and [36], in which the FTN-induced ISI is combined together with the fading channel-induced ISI, we handle them separately by dividing the factor graph into two layers. Hence, the information of the known FTN-induced ISI structure is utilized and the length of FTN-induced ISI considered at the receiver can be truncated practically to substantially reduce the complexity with a negligible performance loss.

- Moreover, we propose a concise LLR representation for the IM scheme in terms of the extrinsic means and variances derived from the message passing algorithm. Furthermore, we propose a two-step low-complexity LLR calculation based on Gaussian mixture model (GMM). By formulating the likelihood function of the signal as a linear mixture corresponding to multiple constellation modes, the time-domain index bits can be determined by a few iterations. Then, symbol set can be restricted to a subset, and the complexity is further reduced especially for systems with large-scale IM symbols.

Simulation results demonstrate the superior bit error rate (BER) performance of the proposed scheme with the same spectral efficiency, as well as the advantages of the proposed GMP-based receiver.

The remainder of this paper is organized as follows. In Section II, we present the system model of STMIM-FTN scheme. In Section III, we propose the GMP-based receiver. The GMM-based low-complexity LLR calculation is devised in Section IV. In Section V, simulation results are shown and discussed. Finally, conclusions are drawn in Section VI.

Notations: Lowercase letters (e.g., x) denote scalars, boldface lowercase letters (e.g., $\mathbf{x}$) denote vectors, and boldface capital letters (e.g., $\mathbf{H}$) denote matrices. The superscripts $(\cdot)^T$, $(\cdot)^H$ and $(\cdot)^{-1}$ denote the transpose, Hermitian, and inverse operations, respectively; $\mathbf{a}_k$ denotes the kth element of $\mathbf{a}$, $\mathbf{a}_{i,k}$ denotes the kth element of $\mathbf{a}_i$, $\mathbf{A}_{k,l}$ denotes the element of $\mathbf{A}$ in the kth row and lth column, and $\mathbf{A}_{:,k}$ denotes the kth column of $\mathbf{A}$; $\mathbf{I}_N$ is an $N \times N$ identity matrix, while $\mathbf{0}_{N\times M}$ is an $N \times M$ all-zero matrix; $\mathbb{Z}$, $\mathbb{R}$, $\mathbb{C}$ and $\varnothing$ are the set of integers, real numbers, complex numbers and null, respectively; $\mathcal{N}(\mu, \sigma^2)$ represents Gaussian distribution with mean μ and variance σ^2; $\propto$ denotes the equality un to a constant factor, $\lfloor\cdot\rfloor$ represents the floor operation, and diag($\mathbf{v}$) represents the diagonal matrix with the diagonal element vector $\mathbf{v}$. Furthermore, $\overrightarrow{\cdot}$ represents the message that passes along the direction of the edge, while $\overleftarrow{\cdot}$ represents the opposite direction message.

II. SYSTEM MODEL

In this section, we present the system model of the proposed STMIM-FTN scheme. As illustrated in Fig. 1, we consider a coded SC-MIMO system with N_t transmit antennas and N_r receive antennas. Note that in the STMIM-FTN scheme, information bits are conveyed by the modulated constellation symbols, the combination pattern of time-domain modulation modes, and the activation pattern of transmit antennas.

A. TRANSMITTER MODEL

In the STMIM-FTN scheme, each index modulation subframe, named as *STMIM symbol*, consists of N_{TI} time-domain slots, i.e. N_{TI} modulation modes. Each time slot contains N_t spatial domain symbols. Hence, the kth transmitted STMIM symbol can be represented by

$$\mathbf{S}_k = \left[\mathbf{s}_{k,1}, \ldots, \mathbf{s}_{k,n}, \ldots, \mathbf{s}_{k,N_{\mathrm{TI}}}\right] \in \mathbb{C}^{N_t \times N_{\mathrm{TI}}}, \tag{1}$$

where $k = 1, 2, \ldots, N_{\mathrm{S}}$, N_{S} is the number of STMIM symbols in one transmission block; $\mathbf{s}_{k,n}$ corresponds to the

nth time slot and is given as

$$\mathbf{s}_{k,n} = [\underbrace{0,\ldots,0}_{I_{k,n}-1}, a_{k,n}, \underbrace{0,\ldots,0}_{N_t-I_{k,n}}]^T \in \mathbb{C}^{N_t\times 1}, \tag{2}$$

$I_{k,n} \in \{i\}_{i=1}^{N_t}$ is the index of the activated transmit antenna in the nth slot of $\mathbf{S}_k$, and $a_{k,n}$ represents the modulated constellation symbols in $\mathbf{s}_{k,n}$. Note that there are N_{TI} modulated symbols in one STMIM symbol, while the others are set to zeros. C bits are transmitted over one STMIM symbol and C can be represented as

$$C = C_{\mathrm{T}} + N_{\mathrm{TI}} \times C_{\mathrm{S}} + \sum_{j=1}^{N_{\mathrm{TI}}} C_{M_j}, \tag{3}$$

where the first C_{T} out of the C bits are referred to as *time-domain index bits*, and they are used for determining the modulation modes of the N_{TI} symbols. More specifically, N_{TI} modulation modes $\{\mathcal{M}_1,\ldots,\mathcal{M}_{N_{\mathrm{TI}}}\}$ are employed by N_{TI} symbols $\{a_{k,1},\ldots,a_{k,N_{\mathrm{TI}}}\}$, where $\mathcal{M}_j$ is an M_j-ary signal constellation with $j \in \{1,\ldots,N_{\mathrm{TI}}\}$. For different time slots, modulation modes should be different. Hence, we have

$$C_{\mathrm{T}} = \lfloor log_2(N_{\mathrm{TI}}!)\rfloor. \tag{4}$$

Moreover, the second part C_{S} out of C bits are referred to as *spatial domain index bits* in each time slot. Consequently, we have

$$C_{\mathrm{S}} = \lfloor log_2(N_t)\rfloor. \tag{5}$$

The third part C_{M_j} bits are used to map the M_j-ary constellation symbol in each time slot, i.e.

$$C_{M_j} = log_2(M_j). \tag{6}$$

Note that the modulation modes $\{\mathcal{M}_1,\ldots,\mathcal{M}_{N_{\mathrm{TI}}}\}$ should not have the same signal constellation point with each other, i.e. $\mathcal{M}_i \cap \mathcal{M}_j = \varnothing$, and the average symbol power should be normalized to unity [14].

As shown in the upper part of the block diagram in Fig. 1, the information bit sequence $\mathbf{b}$ is encoded to an M-length sequence $\mathbf{c}$ with coding rate R_{cc}. Then the encoded bits $\mathbf{c}$ is divided into two parts: $\frac{N_{\mathrm{TI}}\times C_{\mathrm{S}}}{C} \times M$ bits as spatial domain index bits, and the remaining as time-domain MIM bits. The latter part is then serial-to-parallel converted into N_{S} sequences, each sequence contains $C_{\mathrm{T}} + \sum_{j=1}^{N_{\mathrm{TI}}} C_{M_j}$ bits. The first C_{T} bits determine the modulation modes of N_{TI} constellation symbols, whereas the other $\sum_{j=1}^{N_{\mathrm{TI}}} C_{M_j}$ bits are mapped to N_{TI} symbols. After time-domain MIM mapping, N_{TI} constellation symbols of the kth STMIM symbol $\mathbf{S}_k$ are determined as

$$\mathbf{a}_k = [a_{k,1},\ldots,a_{k,n},\ldots,a_{k,N_{\mathrm{TI}}}] \in \mathbb{C}^{1\times N_{\mathrm{TI}}}. \tag{7}$$

At this point, the activation pattern of antennas in $\mathbf{S}_k$, i.e. $I_{k,n}$, is determined by the spatial domain index bits. Then we have the vectorized N-length transmit block $\mathbf{x}$, which can be expressed as

$$\mathbf{x} = [\underbrace{0,\ldots,0}_{I_{1,1}-1}, a_{1,1}, \underbrace{0,\ldots,0}_{N_t-I_{1,1}}, \ldots,$$
$$\underbrace{0,\ldots,0}_{I_{k,n}-1}, a_{k,n}, \underbrace{0,\ldots,0}_{N_t-I_{k,n}}, \ldots,$$
$$\underbrace{0,\ldots,0}_{I_{N_{\mathrm{S}},N_{\mathrm{TI}}}-1}, a_{N_{\mathrm{S}},N_{\mathrm{TI}}}, \underbrace{0,\ldots,0}_{N_t-I_{N_{\mathrm{S}},N_{\mathrm{TI}}}}]^T \in \mathbb{C}^{N\times 1}, \tag{8}$$

where $N = N_t \times N_{\mathrm{S}} \times N_{\mathrm{TI}}$. The symbol block $\mathbf{x}$ is then serial-to-parallel converted into N_t sequences $[\mathbf{x}_1,\ldots,\mathbf{x}_n,\ldots,\mathbf{x}_{N_t}]$, where $n = 1,2,\ldots,N_t$. Each sequence corresponds to its transmit antenna and is passed through the FTN shaping filter, yielding the signal transmitted by the nth antenna

$$s_n(t) = \sum_i g(t - i\tau T_0)\mathbf{x}_{n,i}, \tag{9}$$

where $\mathbf{x}_{n,i}$ is the ith element of $\mathbf{x}_n$, $g(t)$ represents the impulse response of a root-raised-cosine (RRC) filter with roll-off factor β, $0 < \tau < 1$ is the FTN packing factor and T_0 is the symbol period under Nyquist criterion. Finally, the transmission signals are transmitted through N_t antennas.

Based on (3)-(9), the spectral efficiency of the proposed STMIM-FTN system can be given as

$$R = R_{\mathrm{cc}}\frac{1}{\tau}\frac{1}{1+\beta} \times \frac{\lfloor log_2(N_{\mathrm{TI}}!)\rfloor + N_{\mathrm{TI}}\lfloor log_2(N_t)\rfloor + \sum_j log_2(M_j)}{N_{\mathrm{TI}}} \text{bps/Hz}. \tag{10}$$

B. RECEIVER MODEL

As illustrated in Fig. 1, the signal is then transmitted over a frequency selective fading MIMO channel with L_p paths, corrupted by additive white Gaussian noise (AWGN) with power spectral density N_0. Assuming perfect synchronization, the received signal is then matched-filtered with the impulse response $g^*(t)$ and sampled with the symbol rate $\frac{1}{\tau T_0}$. Finally, the N'-length received signal block $\mathbf{r}$, where $N' = N_r \times N_{\mathrm{S}} \times N_{\mathrm{TI}}$, can be represented as

$$\mathbf{r} = \mathbf{H}\mathbf{G_0}\mathbf{x} + \boldsymbol{\xi}, \tag{11}$$

where $\boldsymbol{\xi}$ is the N'-length colored noise vector, $\mathbf{H}$ and $\mathbf{G_0}$ are the matrices with respect to block-fading channel and FTN-induced ISI, respectively. The channel matrix $\mathbf{H}$ is given as

$$\mathbf{H} = \begin{bmatrix} \mathbf{H}_0 & & & & \mathbf{0} \\ \mathbf{H}_1 & \mathbf{H}_0 & & & \\ \vdots & \ddots & & & \\ \mathbf{H}_{L_p-1} & \cdots & \mathbf{H}_0 & & \\ & \ddots & & \ddots & \\ \mathbf{0} & \mathbf{H}_{L_p-1} & \cdots & \mathbf{H}_1 & \mathbf{H}_0 \end{bmatrix} \in \mathbb{R}^{N'\times N}, \tag{12}$$

where $\mathbf{H}_l$ is the $N_r \times N_t$ MIMO channel matrix corresponding to the lth path. The $N \times N$ FTN matrix $\mathbf{G_0}$ is given as

$$\mathbf{G_0} = \begin{bmatrix} g_0 & \mathbf{0}_{N_t'} & g_1 & \mathbf{0}_{N_t'} & g_2 & \cdots & & \\ 0 & g_0 & \mathbf{0}_{N_t'} & g_1 & \mathbf{0}_{N_t'} & g_2 & \cdots & \\ & \ddots & & & & & \ddots & \\ & & \cdots & \mathbf{0}_{N_t'} & g_0 & \mathbf{0}_{N_t'} & \cdots & \\ & & \ddots & & & & & \vdots \\ & & \cdots & g_{-2} & \mathbf{0}_{N_t'} & g_{-1} & \mathbf{0}_{N_t'} & g_0 \end{bmatrix}, \tag{13}$$

where $g_{m-n} = \int g(t - m\tau T_0) g^*(t - n\tau T_0) dt$, $m, n \in \mathbb{Z}$, $\mathbf{0}_{N_t'}$ denotes an all-zero vector $\mathbf{0}_{1\times N_t - 1}$. Note that the FTN signaling results in interference from adjacent symbols with infinite length. However, in the proposed receiver, we choose a sufficiently large L_f as the truncated unilateral interference length considered in the receiver design, leading to the truncated FTN matrix $\mathbf{G}$

$$\mathbf{G} = \begin{bmatrix} g_0 & \mathbf{0}_{N_t'} & g_1 & \cdots & g_{L_f} & & & \mathbf{0} \\ \vdots & & & & & \ddots & & \\ g_{-L_f} & \cdots & \mathbf{0}_{N_t'} & g_0 & \mathbf{0}_{N_t'} & \cdots & g_{L_f} & \\ \ddots & & & & & & \ddots & \\ & g_{-L_f} & \cdots & \mathbf{0}_{N_t'} & g_0 & \mathbf{0}_{N_t'} & \cdots & g_{L_f} \\ & & \ddots & & & & & \vdots \\ \mathbf{0} & & & g_{-L_f} & \cdots & g_{-1} & \mathbf{0}_{N_t'} & g_0 \end{bmatrix}, \tag{14}$$

where L_f is the length of one-side adjacent symbol interference considered at the receiver. It will be shown in Section V via simulation results that as the value of L_f becomes larger, the performance loss induced by the truncation becomes negligible.

III. MESSAGE PASSING RECEIVER DESIGN

In this section, a GMP-based receiver is derived for the proposed STMIM-FTN system.

A. FACTOR GRAPH REPRESENTATION BASED ON STATE-SPACE MODEL

The factor graph representation of the proposed iterative message passing receiver can be illustrated using the state-space model. Define the kth symbol state $\mathbf{z}_k$ as

$$\mathbf{z}_k = [\mathbf{x}_{k-L_f}, \ldots, \mathbf{x}_k, \ldots, \mathbf{x}_{k+L_f}]^T \in \mathbb{C}^{N_t L_{\text{FTN}} \times 1}, \tag{15}$$

where $k = 1, 2, \ldots, N_S \times N_{TI}$, $\mathbf{x}_k$ denotes the N_t-length symbol vector of kth time slot and $L_{\text{FTN}} = 2L_f + 1$. Moreover, the state transition of $\mathbf{z}_k$ is given as

$$\mathbf{z}_{k+1} = \mathbf{A} \cdot \mathbf{z}_k + \mathbf{B} \cdot x_{k+L_f+1}, \tag{16}$$

with $\mathbf{A} = \begin{bmatrix} \mathbf{0}_{N_t(L_{\text{FTN}}-1)\times N_t} & \mathbf{I}_{N_t(L_{\text{FTN}}-1)} \\ \mathbf{0}_{N_t \times N_t} & \mathbf{0}_{N_t \times N_t(L_{\text{FTN}}-1)} \end{bmatrix}$ and $\mathbf{B} = \begin{bmatrix} \mathbf{0}_{N_t(L_{\text{FTN}}-1)\times N_t} \\ \mathbf{I}_{N_t} \end{bmatrix}$. Additionally, we define

$$\mathbf{y}_k = \ddot{\mathbf{G}}^T \cdot \mathbf{z}_k, \tag{17}$$

where

$$\ddot{\mathbf{G}} = \begin{bmatrix} g_{-L_f} & \cdots & \mathbf{0}_{N_t'} & g_0 & \mathbf{0}_{N_t'} & \cdots & g_{L_f} & \\ \ddots & & & & & & \ddots & \\ & g_{-L_f} & \cdots & \mathbf{0}_{N_t'} & g_0 & \mathbf{0}_{N_t'} & \cdots & g_{L_f} \end{bmatrix}^T, \tag{18}$$

which is a $N_t L_{\text{FTN}} \times N_t$ matrix and is obtained from the FTN matrix (14). Note that by defining the expression as (15)-(18), the number of messages passed on the factor graph is reduced substantially. Similarly, we define the state $\mathbf{q_k}$ as

$$\mathbf{q}_k = [\mathbf{y}_{k-L_p+1}, \ldots, \mathbf{y}_{k-1}, \mathbf{y}_k]^T \in \mathbb{C}^{N_t L_p \times 1}. \tag{19}$$

The state transition of $\mathbf{q}_k$ is given as

$$\mathbf{q}_{k+1} = \mathbf{C} \cdot \mathbf{q}_k + \mathbf{D} \cdot \mathbf{y}_{k+1}, \tag{20}$$

where $\mathbf{C} = \begin{bmatrix} \mathbf{0}_{[(N_t(L_p-1))]\times N_t} & \mathbf{I}_{N_t(L_p-1)} \\ \mathbf{0}_{N_t \times N_t} & \mathbf{0}_{N_t \times [N_t(L_p-1)]} \end{bmatrix}$ and $\mathbf{D} = \begin{bmatrix} \mathbf{0}_{[N_t(L_p-1)]\times N_t} \\ \mathbf{I}_{N_t} \end{bmatrix}$. Finally, according to (11) we have

$$\mathbf{r}_k = \ddot{\mathbf{H}}^T \cdot \mathbf{q}_k + \boldsymbol{\xi}_k, \tag{21}$$

where $\mathbf{r}_k$ represents the $(N_r \times (k-1) + 1)$th to $(N_r \times k)$th elements of $\mathbf{r}$, and $\ddot{\mathbf{H}}$ is given as

$$\ddot{\mathbf{H}} = [\mathbf{H}_{L_p-1}, \ldots, \mathbf{H}_0]^T \in \mathbb{R}^{(N_t L_p)\times N_r}. \tag{22}$$

Based on the linear state-space model, given (15)-(22), a Forney-style factor graph can be constructed as depicted in Fig. 2. Note that the Forney-style factor graph only maintains one type of vertex: the *function node*, whereas the variables are represented by the edges. Furthermore, the *equality node* performs exactly as a *variable node* whose representing variable is shared by its neighboring function node.

B. GMP-BASED EQUALIZATION

With Gaussian assumption of messages passing on the factor graph in Fig. 2, the message can be expressed in parametric form, i.e. the GMP scheme. More specifically, the message is characterized by its covariance matrix $\mathbf{V}$ (or the weight matrix $\mathbf{W} = \mathbf{V}^{-1}$) and its mean vector $\mathbf{m}$ (or the transformed mean $\mathbf{Wm}$).[1] Moreover, the model-based GMP algorithm can be efficiently exploited by handling the computation rules of basic building blocks [38]. For ease of exposition, as shown in Fig. 2, we divide the proposed GMP-based receiver into the following four parts: ①the IM bit-to-symbol mapping, ②the FTN equalization, ③the multipath channel equalization and ④the index modulation LLR calculating. Note that the factor graph model in Fig. 2 corresponds to the FTN and multipath equalization part. We detail the message updating scheme in the remainder of this section, whereas the LLR calculation is elaborated in the next subsection.

[1] Due to the sparseness of the transition matrix in our state-space model, either $\mathbf{V}$ or $\mathbf{W}$ is singular for certain messages in some cases [37]. However it is seldom a serious problem, as the singularity can be solved through transforming the message from one parametric form to another owing to the equivalence.

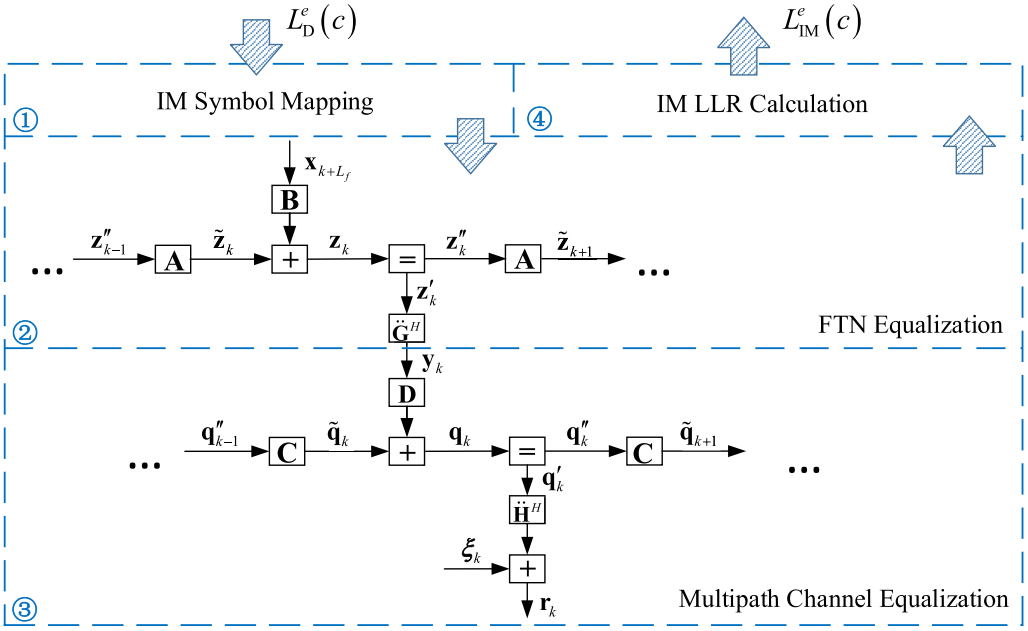

FIGURE 2. Factor graph representation of the proposed message passing receiver.

1) BIT-TO-SYMBOL MAPPING FOR INDEX MODULATION

Provided that the channel decoder output the bit-wise extrinsic LLR as

$$L_{\mathrm{D}}^{e}(c_{n,m}) = \ln\frac{p(c_{n,m}=0)}{p(c_{n,m}=1)}, \tag{23}$$

where $c_{n,m}$ denotes the mth bit of the nth STMIM bit sequence, $n \in \{1,\ldots,N_S\}$ and $m \in \{1,\ldots,C\}$. Define the STMIM symbol set as

$$\boldsymbol{X} = \{\boldsymbol{\chi}_1,\ldots,\boldsymbol{\chi}_k,\ldots,\boldsymbol{\chi}_K\} \in \mathbb{C}^{N_{\mathrm{sym}}\times K}, \tag{24}$$

where $K = 2^C$, $N_{\mathrm{sym}} = N_{\mathrm{t}} \times N_{\mathrm{TI}}$. Obviously, the STMIM symbol set $\boldsymbol{X}$ corresponds to a bit sequence set

$$\boldsymbol{\Psi} = \{\boldsymbol{\psi}_1,\ldots,\boldsymbol{\psi}_k,\ldots,\boldsymbol{\psi}_K\} \in \{0,1\}^{C\times K} \tag{25}$$

with a binary labeling map $\mathcal{F}: \{0,1\}^C \to \boldsymbol{\chi}_k$. Assuming that the information bits are independent, the *a prior* probability of the nth STMIM symbol can be calculated as

$$p_{\tilde{\mathbf{S}}_n=\boldsymbol{\chi}_k} = \prod_{m=1}^{C} p(c_{n,m}=\boldsymbol{\psi}_{k,m}), \tag{26}$$

where $\tilde{\mathbf{S}}_n \in \mathbb{C}^{N_{\mathrm{sym}}\times 1}$ represents the spanned $\mathbf{S}_n$ after vectorization, hence $\tilde{\mathbf{S}}_n \in \boldsymbol{X}$. Define the expanded signal symbol set $\mathcal{A}$ as

$$\mathcal{A} = \{\mathcal{M}_1,\ldots,\mathcal{M}_{N_{TI}}\} \cup \{0\}. \tag{27}$$

Note that the set $\{0\}$ should be considered in the proposed STMIM system due to the existence of "0" symbol in spatial domain. Furthermore, we arrive at the *a priori* probability of symbol x, which is expressed as

$$p_{x=\alpha_j} = \sum_{k=1}^{N_{\mathrm{sym}}} p(\tilde{\mathbf{S}}_n = \boldsymbol{\chi}_k, x=\alpha_j), \tag{28}$$

where x is a symbol of $\tilde{\mathbf{S}}_n$ and $\alpha_j \in \mathcal{A}$. Then the parameters of the input message corresponding to x in the tth iteration can be obtained as

$$\overrightarrow{m}_x^t = \sum_{\alpha_j\in\mathcal{A}} \alpha_j p_{x=\alpha_j}, \tag{29}$$

and

$$\overrightarrow{v}_x^t = \sum_{\alpha_j\in\mathcal{A}} |\alpha_j|^2 p_{x=\alpha_j} - |m_x|^2, \tag{30}$$

Note that the superscript t is omitted in the following part for the sake of brevity.

2) MESSAGE UPDATING FOR FTN EQUALIZER

As shown in Fig. 2 part ②, we start the message updating from the forward to the backward, focusing on the kth state. Provided that parameters $\overrightarrow{\mathbf{m}}_{\tilde{\mathbf{z}}_k}$ and $\overrightarrow{\mathbf{V}}_{\tilde{\mathbf{z}}_k}$ are available (initialize them otherwise), given $\overrightarrow{\mathbf{m}}_{\mathbf{x}_{k+L_f}}$ and $\overrightarrow{\mathbf{V}}_{\mathbf{x}_{k+L_f}}$ from the IM bit-to-symbol mapping, we have

$$\overrightarrow{\mathbf{V}}_{\mathbf{z}_k} = \overrightarrow{\mathbf{V}}_{\tilde{\mathbf{z}}_k} + \mathbf{B}\overrightarrow{\mathbf{V}}_{\mathbf{x}_{k+L_f}}\mathbf{B}^H, \tag{31}$$

$$\overrightarrow{\mathbf{m}}_{\mathbf{z}_k} = \overrightarrow{\mathbf{m}}_{\tilde{\mathbf{z}}_k} + \mathbf{B}\overrightarrow{\mathbf{m}}_{\mathbf{x}_{k+L_f}}. \tag{32}$$

Then $\overrightarrow{\mathbf{V}}_{\mathbf{z}''_k}$ and $\overrightarrow{\mathbf{m}}_{\mathbf{z}''_k}$ can be obtained as

$$\overrightarrow{\mathbf{V}}_{\mathbf{z}''_k} = \overrightarrow{\mathbf{V}}_{\mathbf{z}_k} - \overrightarrow{\mathbf{V}}_{\mathbf{z}_k}\ddot{\mathbf{G}}\mathbf{K}\ddot{\mathbf{G}}^H\overrightarrow{\mathbf{V}}_{\mathbf{z}_k}, \tag{33}$$

$$\overrightarrow{\mathbf{m}}_{\mathbf{z}''_k} = \overrightarrow{\mathbf{m}}_{\mathbf{z}_k} + \overrightarrow{\mathbf{V}}_{\mathbf{z}_k}\ddot{\mathbf{G}}\mathbf{K}\Big(\overleftarrow{\mathbf{m}}_{\mathbf{y}_k} - \ddot{\mathbf{G}}^H\overrightarrow{\mathbf{m}}_{\mathbf{z}_k}\Big), \tag{34}$$

where

$$\mathbf{K} = \Big(\overleftarrow{\mathbf{W}}_{\mathbf{y}_k} + \ddot{\mathbf{G}}^H\overrightarrow{\mathbf{V}}_{\mathbf{z}_k}\ddot{\mathbf{G}}\Big)^{-1}, \tag{35}$$

and $\overleftarrow{\mathbf{W}}_{\mathbf{y}_k}$, $\overleftarrow{\mathbf{m}}_{\mathbf{y}_k}$ denote the upward messages from the lower part. Additionally, the $\overrightarrow{\mathbf{V}}_{\tilde{\mathbf{z}}_{k+1}}$ and $\overrightarrow{\mathbf{m}}_{\tilde{\mathbf{z}}_{k+1}}$ for the next state are given as

$$\overrightarrow{\mathbf{V}}_{\tilde{\mathbf{z}}_{k+1}} = \mathbf{A}\overrightarrow{\mathbf{V}}_{\mathbf{z}''_k}\mathbf{A}^H, \tag{36}$$

$$\overrightarrow{\mathbf{m}}_{\tilde{\mathbf{z}}_{k+1}} = \mathbf{A}\overrightarrow{\mathbf{m}}_{\mathbf{z}''_k}. \tag{37}$$

Similarly, the backward messages can be obtained as

$$\overleftarrow{\mathbf{W}}_{\mathbf{z}_k} = \overleftarrow{\mathbf{W}}_{\mathbf{z}''_k} + \ddot{\mathbf{G}}\overleftarrow{\mathbf{W}}_{\mathbf{y}_k}\ddot{\mathbf{G}}^H, \tag{38}$$

$$\overleftarrow{\mathbf{W}}_{\mathbf{z}_k}\overleftarrow{\mathbf{m}}_{\mathbf{z}_k} = \overleftarrow{\mathbf{W}}_{\mathbf{z}''_k}\overleftarrow{\mathbf{m}}_{\mathbf{z}''_k} + \ddot{\mathbf{G}}\overleftarrow{\mathbf{W}}_{\mathbf{y}_k}\overleftarrow{\mathbf{m}}_{\mathbf{y}_k}, \tag{39}$$

and

$$\overleftarrow{\mathbf{W}}_{\tilde{\mathbf{z}}_k} = \overleftarrow{\mathbf{W}}_{\mathbf{z}_k} - \overleftarrow{\mathbf{W}}_{\mathbf{z}_k}\mathbf{B}\mathbf{M}\mathbf{B}^H\overleftarrow{\mathbf{W}}_{\mathbf{z}_k}, \tag{40}$$

$$\begin{aligned}\overleftarrow{\mathbf{W}}_{\tilde{\mathbf{z}}_k}\overleftarrow{\mathbf{m}}_{\tilde{\mathbf{z}}_k} = &\Big(\mathrm{I}_{L_{\mathrm{FTN}}} - \overleftarrow{\mathbf{W}}_{\mathbf{z}_k}\mathbf{B}\mathbf{M}\mathbf{B}^H\Big)\\ &\cdot\Big(\overleftarrow{\mathbf{W}}_{\mathbf{z}_k}\overleftarrow{\mathbf{m}}_{\mathbf{z}_k} - \overleftarrow{\mathbf{W}}_{\mathbf{z}_k}\mathbf{B}\overrightarrow{\mathbf{m}}_{\mathbf{x}_{k+L_f}}\Big),\end{aligned} \tag{41}$$

where

$$\mathbf{M} = \Big(\overrightarrow{\mathbf{V}}^{-1}_{\mathbf{x}_{k+L_f}} + \mathbf{B}^H\overleftarrow{\mathbf{W}}_{\mathbf{z}_k}\mathbf{B}\Big)^{-1}. \tag{42}$$

Then the parameters for the next backward state are given as

$$\overleftarrow{\mathbf{W}}_{\mathbf{z}''_{k-1}} = \mathbf{A}^H\overleftarrow{\mathbf{W}}_{\tilde{\mathbf{z}}_k}\mathbf{A}, \tag{43}$$

$$\overleftarrow{\mathbf{W}}_{\mathbf{z}''_{k-1}}\overleftarrow{\mathbf{m}}_{\mathbf{z}''_{k-1}} = \mathbf{A}^H\overleftarrow{\mathbf{W}}_{\tilde{\mathbf{z}}_k}\overleftarrow{\mathbf{m}}_{\tilde{\mathbf{z}}_k}. \tag{44}$$

Finally, the downward message, which is passed to the multipath channel equalizer, can be characterized by

$$\overrightarrow{\mathbf{V}}_{\mathbf{y}_k} = \ddot{\mathbf{G}}^H\overrightarrow{\mathbf{V}}_{\mathbf{z}'_k}\ddot{\mathbf{G}}, \tag{45}$$

and

$$\overrightarrow{\mathbf{m}}_{\mathbf{y}_k} = \ddot{\mathbf{G}}^H\overrightarrow{\mathbf{m}}_{\mathbf{z}'_k}, \tag{46}$$

where $\overrightarrow{\mathbf{V}}_{\mathbf{z}'_k}$ and $\overrightarrow{\mathbf{m}}_{\mathbf{z}'_k}$ are given as

$$\overrightarrow{\mathbf{V}}_{\mathbf{z}'_k} = \Big(\overrightarrow{\mathbf{V}}^{-1}_{\mathbf{z}_k} + \overleftarrow{\mathbf{W}}_{\mathbf{z}''_k}\Big)^{-1}, \tag{47}$$

and

$$\overrightarrow{\mathbf{m}}_{\mathbf{z}'_k} = \overrightarrow{\mathbf{V}}_{\mathbf{z}'_k}\Big(\overrightarrow{\mathbf{V}}^{-1}_{\mathbf{z}_k}\overrightarrow{\mathbf{m}}_{\mathbf{z}_k} + \overleftarrow{\mathbf{W}}_{\mathbf{z}''_k}\overleftarrow{\mathbf{m}}_{\mathbf{z}''_k}\Big). \tag{48}$$

3) MESSAGE UPDATING FOR MULTIPATH CHANNEL EQUALIZER

In a similar way, we concentrate on the message updating in the Fig. 2 part ③, i.e. the multipath channel equalizer. The parameters $\overrightarrow{\mathbf{V}}_{\mathbf{q}_k}$ and $\overrightarrow{\mathbf{m}}_{\mathbf{q}_k}$ can be expressed as

$$\overrightarrow{\mathbf{V}}_{\mathbf{q}_k} = \overrightarrow{\mathbf{V}}_{\tilde{\mathbf{q}}_k} + \mathbf{D}\overrightarrow{\mathbf{V}}_{\mathbf{y}_k}\mathbf{D}^H, \tag{49}$$

$$\overrightarrow{\mathbf{m}}_{\mathbf{q}_k} = \overrightarrow{\mathbf{m}}_{\tilde{\mathbf{q}}_k} + \mathbf{D}\overrightarrow{\mathbf{m}}_{\mathbf{y}_k}, \tag{50}$$

then we arrive at

$$\overrightarrow{\mathbf{V}}_{\mathbf{q}''_k} = \overrightarrow{\mathbf{V}}_{\mathbf{q}_k} - \overrightarrow{\mathbf{V}}_{\mathbf{q}_k}\ddot{\mathbf{H}}\mathbf{Q}\ddot{\mathbf{H}}^H\overrightarrow{\mathbf{V}}_{\mathbf{q}_k}, \tag{51}$$

$$\overrightarrow{\mathbf{m}}_{\mathbf{q}''_k} = \overrightarrow{\mathbf{m}}_{\mathbf{q}_k} + \overrightarrow{\mathbf{V}}_{\mathbf{q}_k}\ddot{\mathbf{H}}\mathbf{Q}\Big(\mathbf{r}_k - \ddot{\mathbf{H}}^H\overrightarrow{\mathbf{m}}_{\mathbf{q}_k}\Big), \tag{52}$$

where

$$\mathbf{Q} = \Big(N_0\mathbf{I}_{N_t} + \ddot{\mathbf{H}}^H\overrightarrow{\mathbf{V}}_{\mathbf{q}_k}\ddot{\mathbf{H}}\Big)^{-1}. \tag{53}$$

Meanwhile, $\overrightarrow{\mathbf{V}}_{\tilde{\mathbf{q}}_{k+1}}$ and $\overrightarrow{\mathbf{m}}_{\tilde{\mathbf{q}}_{k+1}}$ for the next state $\mathbf{q}_{k+1}$ are given as

$$\overrightarrow{\mathbf{V}}_{\tilde{\mathbf{q}}_{k+1}} = \mathbf{C}\overrightarrow{\mathbf{V}}_{\mathbf{q}''_k}\mathbf{C}^H, \tag{54}$$

$$\overrightarrow{\mathbf{m}}_{\tilde{\mathbf{q}}_{k+1}} = \mathbf{C}\overrightarrow{\mathbf{m}}_{\mathbf{q}''_k}. \tag{55}$$

Similarly, the backward messages can be obtained in a similar way. For the state $\mathbf{q}_k$, we have

$$\overleftarrow{\mathbf{W}}_{\mathbf{q}_k} = \overleftarrow{\mathbf{W}}_{\mathbf{q}''_k} + \frac{\ddot{\mathbf{H}}\ddot{\mathbf{H}}^H}{N_0}, \tag{56}$$

$$\overleftarrow{\mathbf{W}}_{\mathbf{q}_k}\overleftarrow{\mathbf{m}}_{\mathbf{q}_k} = \overleftarrow{\mathbf{W}}_{\mathbf{q}''_k}\overleftarrow{\mathbf{m}}_{\mathbf{q}''_k} + \frac{\ddot{\mathbf{H}}\mathbf{r}_k}{N_0}. \tag{57}$$

Then $\overleftarrow{\mathbf{V}}_{\tilde{\mathbf{q}}_k}$ and $\overleftarrow{\mathbf{m}}_{\tilde{\mathbf{q}}_k}$ are given as

$$\overleftarrow{\mathbf{V}}_{\tilde{\mathbf{q}}_k} = \overleftarrow{\mathbf{V}}_{\mathbf{q}_k} + \mathbf{D}\overrightarrow{\mathbf{V}}_{\mathbf{y}_k}\mathbf{D}, \tag{58}$$

$$\overleftarrow{\mathbf{m}}_{\tilde{\mathbf{q}}_k} = \overleftarrow{\mathbf{m}}_{\mathbf{q}_k} + \mathbf{D}\overrightarrow{\mathbf{m}}_{\mathbf{y}_k}. \tag{59}$$

Finally, for the next backward state $\mathbf{q}''_{k-1}$, we have

$$\overleftarrow{\mathbf{W}}_{\mathbf{q}''_{k-1}} = \mathbf{C}^H\overleftarrow{\mathbf{V}}^{-1}_{\tilde{\mathbf{q}}_k}\mathbf{C}, \tag{60}$$

$$\overleftarrow{\mathbf{W}}_{\mathbf{q}''_{k-1}}\overleftarrow{\mathbf{m}}_{\mathbf{q}''_{k-1}} = \mathbf{C}^H\overleftarrow{\mathbf{V}}^{-1}_{\tilde{\mathbf{q}}_k}\overleftarrow{\mathbf{m}}_{\tilde{\mathbf{q}}_k}. \tag{61}$$

Furthermore, the upward message corresponding to $\mathbf{y}_{k+l}$ from the lower part to the upper part of the factor graph can be characterized as

$$\overleftarrow{\mathbf{W}}_{q_k} = \mathbf{D}^H\Big(\overrightarrow{\mathbf{V}}_{\tilde{\mathbf{q}}_k} + \overleftarrow{\mathbf{V}}_{\mathbf{q}_k}\Big)^{-1}\mathbf{D}, \tag{62}$$

$$\overleftarrow{\mathbf{W}}_{q_k}\overleftarrow{\mathbf{m}}_{q_k} = \mathbf{D}^H\Big(\overrightarrow{\mathbf{V}}_{\tilde{\mathbf{q}}_k} + \overleftarrow{\mathbf{V}}_{\mathbf{q}_k}\Big)^{-1}\Big(\overleftarrow{\mathbf{m}}_{\mathbf{q}_k} - \overrightarrow{\mathbf{m}}_{\mathbf{q}_k}\Big). \tag{63}$$

C. LLR CALCULATION FOR INDEX MODULATION

After all the messages are computed in Fig. 2 from downward to upward, the outgoing message of symbol $\mathbf{x}_{k+L_f}$ can be parameterized by

$$\overleftarrow{\mathbf{V}}_{\mathbf{x}_{k+L_f}} = \Big(\mathbf{B}^H\Big(\overrightarrow{\mathbf{V}}_{\tilde{\mathbf{z}}_k} + \overleftarrow{\mathbf{V}}_{\mathbf{z}_k}\Big)^{-1}\mathbf{B}\Big)^{-1}, \tag{64}$$

and

$$\overleftarrow{\mathbf{m}}_{\mathbf{x}_{k+L_f}} = \overleftarrow{\mathbf{V}}_{\mathbf{x}_{k+L_f}}\cdot\Big(\mathbf{B}^H\big(\overrightarrow{\mathbf{V}}_{\tilde{\mathbf{z}}_k} + \overleftarrow{\mathbf{V}}_{\mathbf{z}_k}\big)^{-1}\big(\overleftarrow{\mathbf{m}}_{\mathbf{z}_k} - \overrightarrow{\mathbf{m}}_{\tilde{\mathbf{z}}_k}\big)\Big). \tag{65}$$

The extrinsic LLR $L^e_{\mathrm{IM}}(c_{n,m})$ of code bit $c_{n,m}$ passed from the IM equalizer to the channel decoder is calculated based on the soft information of each symbol. Note that STMIM symbol $\mathbf{S}$ is the basic unit to convey information in the proposed STMIM system, which is different from the conventional system whose basic unit is essentially constellation symbol x.

Consequently, the extrinsic LLR should be calculated through $\mathbf{S}$ rather than x. According to turbo principle, we have

$$L_{\mathrm{IM}}^{e}(c_{n,m}) = \ln\frac{p(c_{n,m}=0|\mathbf{r})}{p(c_{n,m}=1|\mathbf{r})} - L_{\mathrm{D}}^{e}(c_{n,m}) = \ln\frac{\sum\limits_{\boldsymbol{\lambda}_i\in\boldsymbol{\chi}_m^0} p(\mathbf{r}|\tilde{\mathbf{S}}_n=\boldsymbol{\lambda}_i)\prod\limits_{m'\neq m} p_{\mathrm{D}}(c_{n,m'}=\psi_{n,m'})}{\sum\limits_{\boldsymbol{\lambda}_i\in\boldsymbol{\chi}_m^1} p(\mathbf{r}|\tilde{\mathbf{S}}_n=\boldsymbol{\lambda}_i)\prod\limits_{m'\neq m} p_{\mathrm{D}}(c_{n,m'}=\psi_{n,m'})}, \tag{66}$$

where $L_{\mathrm{D}}^{e}(c_{n,m})$ represents the extrinsic LLR from channel decoder in the previous turbo iteration; $\boldsymbol{\chi}_m^0$ and $\boldsymbol{\chi}_m^1$ represent the set of $\boldsymbol{\chi}_k \in \boldsymbol{X}$ whose corresponded bit sequence $\boldsymbol{\psi}_k$'s mth element $\psi_{k,m}$ equals 0 and 1, respectively. Recall that $\boldsymbol{X}$ is the STMIM symbol set and $\boldsymbol{\Psi}$ is the corresponded bit sequence set. Assuming the independence between elements of $\tilde{\mathbf{S}}_n$, the likelihood function in (66) can be factorized as

$$p(\mathbf{r}|\tilde{\mathbf{S}}_n=\boldsymbol{\lambda}_i) = \prod_{l=1}^{N_{\mathrm{sym}}} p(\mathbf{r}|\tilde{\mathbf{S}}_{n,l}=\lambda_{i,l}), \tag{67}$$

where $\lambda_{i,l}$ represents the lth symbol of $\boldsymbol{\lambda}_i$ and $l = 1, 2, \ldots, N_{\mathrm{sym}}$. Considering the factor $p(\mathbf{r}|\tilde{\mathbf{s}}_{n,l}=\lambda_{i,l})$, given the Gaussian parameters of $\tilde{\mathbf{S}}_{n,l}$, i.e. $\overleftarrow{m}_{n,l}$ and $\overleftarrow{v}_{n,l}$ from (64) and (65), a concise representation of the symbol-wise likelihood function can be expressed as [39]

$$p(\mathbf{r}|\tilde{\mathbf{S}}_{n,l}=\lambda_{i,l}) = \frac{1}{\pi\overleftarrow{v}_{n,l}}\exp\left(-\frac{(\lambda_{i,l}-\overleftarrow{m}_{n,l})^2}{\overleftarrow{v}_{n,l}}\right). \tag{68}$$

Consequently, (67) can be rewritten as

$$p(\mathbf{r}|\tilde{\mathbf{S}}_n=\boldsymbol{\lambda}_i) = \frac{\exp\left(-\frac{1}{2}(\mathbf{m}_n-\boldsymbol{\lambda}_i)^T\mathbf{V}_n^{-1}(\mathbf{m}_n-\boldsymbol{\lambda}_i)\right)}{\pi^{N_{\mathrm{sym}}}\prod_l v_{n,l}}, \tag{69}$$

where $\mathbf{V}_n$ and $\mathbf{m}_n$ denote the Gaussian parameters of $\tilde{\mathbf{S}}_n$. Finally, by substituting (67)-(69) into (66), $L_{\mathrm{IM}}^{e}(c_{n,m})$ can be expressed as

$$L_{\mathrm{IM}}^{e}(c_{n,m}) = \ln\frac{\sum\limits_{\boldsymbol{\lambda}_i\in\boldsymbol{\chi}_m^0}\exp(\mathbf{m}_n,\mathbf{V}_n,\boldsymbol{\lambda}_i)\prod\limits_{m'\neq m}p_{\mathrm{D},m'}}{\sum\limits_{\boldsymbol{\lambda}_i\in\boldsymbol{\chi}_m^1}\exp(\mathbf{m}_n,\mathbf{V}_n,\boldsymbol{\lambda}_i)\prod\limits_{m'\neq m}p_{\mathrm{D},m'}}, \tag{70}$$

where $\exp\left(-\frac{1}{2}(\mathbf{m}_n-\boldsymbol{\lambda}_i)^T\mathbf{V}_n^{-1}(\mathbf{m}_n-\boldsymbol{\lambda}_i)\right)$ and $p_{\mathrm{D}}(c_{n,m'}=\psi_{n,m'})$ are briefly denoted by $\exp(\mathbf{m}_n,\mathbf{V}_n,\boldsymbol{\lambda}_i)$ and $p_{\mathrm{D},m'}$, respectively.

We summarize the details of the proposed GMP-based receiver for IM system in **Algorithm 1**.

D. COMPLEXITY ANALYSIS

The computational complexity of the proposed GMP algorithm is dominated by matrix inverse operations in (47)-(48), (53) and (60)-(65). It is known that the complexity of inverse operation for a non-sparse $L \times L$ matrix is $\mathcal{O}(L^3)$, where $\mathcal{O}$ denotes the order of complexity. As for (47)-(48), which is related to the FTN equalization, the complexity of inverse operation is $\mathcal{O}(N \times (N_t \times L_{\mathrm{FTN}})^3)$ per transmission block per iteration. In terms of the channel equalizer, the complexity of (53) and (60)-(65) is $\mathcal{O}(N \times (N_t \times L_p)^3)$. Hence, the total computational complexity of the proposed GMP algorithm is $\mathcal{O}\big(N\big((N_t L_{\mathrm{FTN}})^3 + (N_t L_p)^3\big)\big)$ per transmission block per iteration, which increases linearly with the block length N. Note that in practice, a sufficiently large L_{FTN} can be chosen at the receiver as the truncated unilateral interference length with negligible performance loss, which can be much smaller than L_p. As a comparison, the computational complexity of the detectors in [40], the factor graph-based two-step detector in [21] and Gaussian soft interference cancellation are all $\mathcal{O}(N^3)$.

Algorithm 1 The Proposed GMP-Based Iterative Receiver for FTN-Aided STMIM System Over Frequency Selective Channels

1: **Initialization**:
The extrinsic LLR from channel decoder in the first iteration is initialized as $L_{\mathrm{D}}^{0}(c_{n,m}) = 0$.
2: **Entering** turbo iteration
3: **for** $t = 1$ to I_{turbo} **do**
4: Mapping the IM symbols according to (29) and (30);
5: Calculate the messages from FTN equalizer to multi-path channel equalizer according to (45) and (46);
6: Calculate the messages from multipath channel equalizer back to FTN equalizer according to (62) and (63);
7: **for** $n = 1$ to N_{S} **do**
8: Calculate the IM equalization extrinsic LLR $L_{\mathrm{IM}}^{e}(c_{n,m})$ according to (70);
9: **end for**
10: Perform channel decoding algorithm and output the extrinsic LLR $L_{\mathrm{D}}^{t+1}(c_{n,m})$ to equalizer.
11: **end for**
12: Decision of data bits.

IV. LOW-COMPLEXITY LLR CALCULATION BASED ON GMM

In this section, we develop a low-complexity LLR calculation method for the proposed STMIM-FTN scheme. More specifically, a GMM-based likelihood function is considered to replace the likelihood function in (70). By updating the weights of each GMM components with a few iterations, the modulation modes of time slots can be determined, resulting in a substantial reduction of the STMIM symbol sets.

Recall that in the kth STMIM symbol $\mathbf{S}_k$, N_{TI} modulation modes $\{\mathcal{M}_1, \ldots, \mathcal{M}_{N_{\mathrm{TI}}}\}$ are employed by N_{TI} constellation symbols $[a_{k,1}, \ldots, a_{k,n}, \ldots, a_{k,N_{\mathrm{TI}}}]$. Divide the STMIM symbol set $\boldsymbol{X}$ into $2^{C_{\mathrm{T}}}$ subsets

$$\boldsymbol{X} = \boldsymbol{X}_1 \cup \ldots \cup \boldsymbol{X}_l \cup \ldots \cup \boldsymbol{X}_{2^{C_{\mathrm{T}}}}, \tag{71}$$

where $\boldsymbol{X}_l \in \mathbb{C}^{N_{\mathrm{sym}}\times 2^{C-C_{\mathrm{T}}}}$ denotes a subset of $\boldsymbol{X}$ corresponding to a single combination of time-domain modulation modes, and $\boldsymbol{X}_1 \cap \ldots \cap \boldsymbol{X}_l \cap \ldots \cap \boldsymbol{X}_{2^{C_{\mathrm{T}}}} = \varnothing$ is satisfied. Once the combination of modulation modes is determined,

the STMIM symbol set $\boldsymbol{X}$ in (70) can be replaced by a certain subset $\boldsymbol{X}_l$, reducing the computational complexity of LLR calculation.

Consider $\exp(\mathbf{m}_n, \mathbf{V}_n, \boldsymbol{\lambda}_i)$ as a linear combination of 2^{C_T} Gaussian probability density functions, i.e. the Gaussian mixture model

$$\exp(\mathbf{m}_n, \mathbf{V}_n, \boldsymbol{\lambda}_i) = \sum_{l=1}^{2^{C_\mathrm{T}}} \pi_{\boldsymbol{X}_l} \exp(\mathbf{m}_n, \mathbf{V}_n, \boldsymbol{\lambda}_i^l), \tag{72}$$

where $\boldsymbol{\lambda}_i^l \in \boldsymbol{X}_l$. The *mixing coefficient* $\pi_{\boldsymbol{X}_l}$ in GMM can be regarded as the *a priori* probability of the lth component $\exp(\mathbf{m}_n, \mathbf{V}_n, \boldsymbol{\lambda}_i^l)$, and satisfies $\sum_l \pi_{\boldsymbol{X}_l} = 1$. Using Bayes' theorem, the *a posteriori* probability of $\tilde{\mathbf{S}}_n \in \boldsymbol{X}_l$ can be obtained as [12]

$$p(\tilde{\mathbf{S}}_n \in \boldsymbol{X}_l | \mathbf{r}) \propto p(\tilde{\mathbf{S}}_n \in \boldsymbol{X}_l) p(\mathbf{r} | \tilde{\mathbf{S}}_n \in \boldsymbol{X}_l). \tag{73}$$

Substitute $p(\tilde{\mathbf{S}}_n \in \boldsymbol{X}_l)$ in (73) by $\pi_{\boldsymbol{X}_l}^{t-1}$ which is obtained in the $(t-1)$th iteration and we arrive at

$$p(\tilde{\mathbf{S}}_n \in \boldsymbol{X}_l | \mathbf{r}) \propto \pi_{\boldsymbol{X}_l}^{t-1} \sum_{\boldsymbol{\lambda}_i \in \boldsymbol{X}_l} \frac{\exp(\mathbf{m}_n, \mathbf{V}_n, \boldsymbol{\lambda}_i^l)}{\pi^{N_\mathrm{sym}} \prod_l v_{n,l}}. \tag{74}$$

Then we obtain the mixing coefficient of the tth iteration, i.e. $\pi_{\boldsymbol{X}_l}^t$, as

$$\pi_{\boldsymbol{X}_l}^t = \frac{p(\tilde{\mathbf{S}}_n \in \boldsymbol{X}_l | \mathbf{r})}{\sum_{l=1}^{2^{C_\mathrm{T}}} p(\tilde{\mathbf{S}}_n \in \boldsymbol{X}_l | \mathbf{r})}. \tag{75}$$

According to (72)-(75), the GMM-based extrinsic LLR is given as

$$L_{\mathrm{GMM}}^e(c_{n,m}) = \ln \frac{\sum_{\boldsymbol{\lambda}_i \in \boldsymbol{X}_l^0} \sum_{l=1}^{2^{C_\mathrm{T}}} \pi_{\boldsymbol{X}_l} \exp(\mathbf{m}_n, \mathbf{V}_n, \boldsymbol{\lambda}_i^l) \prod_{m' \neq m} p_{\mathrm{D},m'}}{\sum_{\boldsymbol{\lambda}_i \in \boldsymbol{X}_l^1} \sum_{l=1}^{2^{C_\mathrm{T}}} \pi_{\boldsymbol{X}_l} \exp(\mathbf{m}_n, \mathbf{V}_n, \boldsymbol{\lambda}_i^l) \prod_{m' \neq m} p_{\mathrm{D},m'}}. \tag{76}$$

Note that the exponent $\exp(\mathbf{m}_n, \mathbf{V}_n, \boldsymbol{\lambda}_i^l)$ calculated in (74) can be reused in (76), which avoids complexity increase compared with (70). Furthermore, after I_{GMM} iterations, where I_{GMM} is much smaller than I_{turbo}, we consider that the combination of modulation modes is determined according to $\pi_{\boldsymbol{X}_l}^{I_{\mathrm{GMM}}}$, leading to

$$L_{\mathrm{GMM}}^e(c_{n,m}) = \ln \frac{\sum_{\boldsymbol{\lambda}_i \in \boldsymbol{X}_{l_M}^0} \exp(\mathbf{m}_n, \mathbf{V}_n, \boldsymbol{\lambda}_i) \prod_{m' \neq m} p_{\mathrm{D},m'}}{\sum_{\boldsymbol{\lambda}_i \in \boldsymbol{X}_{l_M}^1} \exp(\mathbf{m}_n, \mathbf{V}_n, \boldsymbol{\lambda}_i) \prod_{m' \neq m} p_{\mathrm{D},m'}}, \tag{77}$$

where

$$\boldsymbol{X}_{l_M} = \arg\max_{\boldsymbol{X}_l} \pi_{\boldsymbol{X}_l}^{I_{\mathrm{GMM}}} \tag{78}$$

It can be seen that the STMIM symbol set $\boldsymbol{X}$ in (70) is replaced by $\boldsymbol{X}_{l_M}$ in (77), which is much smaller than the former. As a further comment, this reduction results from the determination of modulation modes combination in the first I_{GMM} iterations. Hence, the GMM-based calculation is a two-step method in a sense. However, distinguished from the two-step detector with hard decision in [21] *et al.*, the proposed GMM-based method updates the *soft* probability of modulation modes, i.e. $\pi_{\boldsymbol{X}_l}$, during the first I_{GMM} iterations. Consequently, the computational complexity can be further decreased in the GMM-based method along with a better performance than the conventional two-step hard-decision methods. It will be shown in simulation results that the proposed GMM-based LLR calculation only exhibits slight performance loss with a small I_{GMM}.

Finally, we evaluate the complexity of GMM-based LLR calculation in terms of the floating point (FLOP) operations and compare it with the conventional method. Note that the multiplication of two complex number needs six FLOPs, $\exp(\cdot)$ and $\log(\cdot)$ can be operated through a look-up table. Hence, calculation in (70) needs around $2^C N_\mathrm{S}(18 N_\mathrm{TI} N_t + 2^{C-1})$ FLOPs per transmission block per iteration, whereas (77) needs $2^C N_\mathrm{S}(18 N_t + 2^{C-1}/N_\mathrm{TI}^2)$ FLOPs. Consequently, the GMM-based LLR calculation is able to further reduce the computational complexity of the proposed receiver.

We summarize the details of the proposed GMP-GMM algorithm in **Algorithm 2**.

Algorithm 2 The Proposed GMP-Based Iterative Receiver With GMM for FTN-Aided STMIM System Over Frequency Selective Channels

1: **Initialization**:
   The extrinsic LLR from channel decoder in the first iteration is initialized as $L_\mathrm{D}^0(c_{n,m}) = 0$.
2: **Entering** turbo iteration
3: **for** $t = 1$ to I_{turbo} **do**
4: Mapping the IM symbols according to (29) and (30);
5: Calculate the messages from FTN equalizer to multipath channel equalizer according to (45) and (46);
6: Calculate the messages from multipath channel equalizer back to FTN equalizer according to (62) and (63);
7: **if** $t \leq I_{\mathrm{GMM}}$ **then**
8: Calculate the GMM-based IM equalization extrinsic LLR $L_{\mathrm{IM}}^e(c_{n,m})$ according to (76);
9: **else**
10: Calculate the GMM-based IM equalization extrinsic LLR $L_{\mathrm{IM}}^e(c_{n,m})$ according to (77) ;
11: **end if**
12: Perform channel decoding algorithm and output the extrinsic LLR $L_\mathrm{D}^{t+1}(c_{n,m})$ to equalizer.
13: **end for**
14: Decision of data bits.

V. SIMULATION RESULTS

In this section, we evaluate the proposed STMIM-FTN system and GMP-based receiver by Monte Carlo simulation. Consider a low-density parity-check (LDPC) coded system

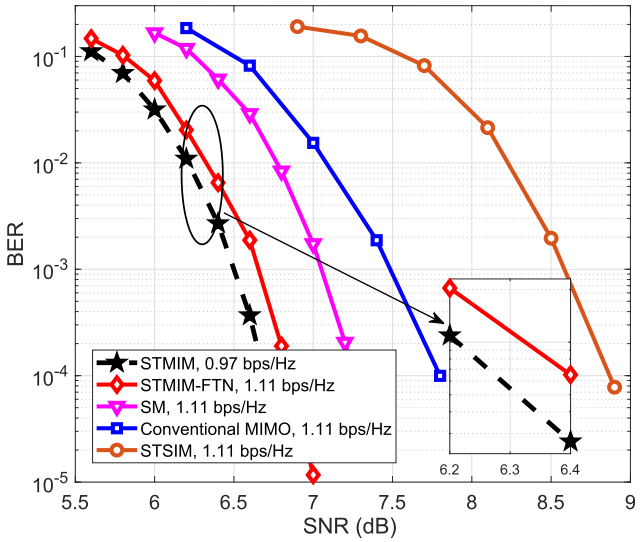

FIGURE 3. BER performance of different systems with spectral efficiency 0.97 bps/Hz and 1.11 bps/Hz.

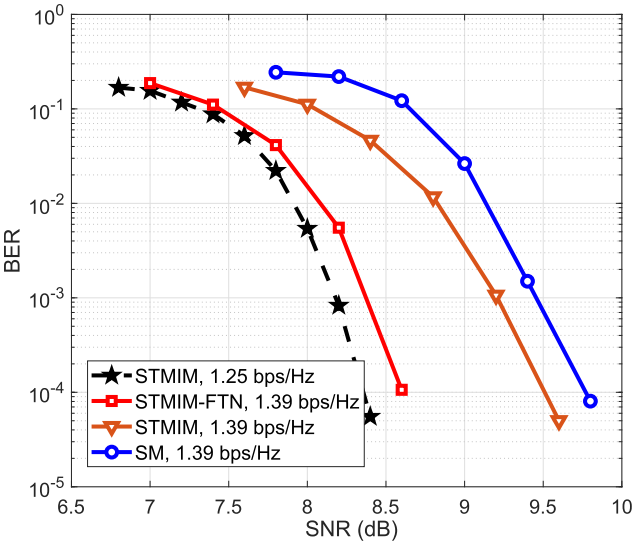

FIGURE 4. BER performance of different systems with spectral efficiency 1.25 bps/Hz and 1.39 bps/Hz.

with coding rate $R_{\rm cc} = 1/2$ and the maximum number of decoding iteration $I = 50$. The number of transmitted symbols in a block is $N = 4608$. A RRC shaping filter is employed with the roll-off factor $\beta = 0.8$. The number of antennas is $N_t = N_r = 4$. The frequency selective fading MIMO channel is assumed to obtain $L_p = 8$ taps and each $N_r \times N_t$ channel block $\mathbf{H}_l$ in (12) is independently generated according to the distribution $\mathbf{h}_{i,j}^l \sim \mathcal{N}(0, d^l)$, where $\mathbf{h}_{i,j}^l$ is the element in the ith row jth column of $\mathbf{H}_l$, and the power delay coefficient $d^l = \exp(-0.05l)$. The number of iterations of turbo equalization is set to $I_{\rm turbo} = 15$, unless otherwise specified.[2]

The BER performance versus the signal-to-noise ratio (SNR) of several multi-antenna schemes with and without IM over the same channel is shown in Fig. 3 and Fig. 4, including the proposed STMIM-FTN system. In Fig. 3, the STMIM and STMIM-FTN schemes have the following parameters: $\{N_{\rm TI}, N_{\rm t}; (M_1, \ldots, M_j)\} = \{2, 4; (2, 2)\}$, $\mathcal{M}_1 = \{+1, -1\}$, $\mathcal{M}_2 = \{+j, -j\}$. Moreover, the FTN packing factor of the STMIM-FTN scheme is $\tau = 0.875$ and L_f is set to 5. For the conventional SM scheme, a QPSK constellation alphabet is utilized for modulating, and one out of N_t antennas is selected by index bits to convey the constellated symbol. In the space-time SIM (STSIM) scheme, one slot is selected out of each two slots to transmit a 2^Q-PSK modulated symbol with $Q = 5$. The conventional MIMO employs a BPSK signal constellation, and all antennas transmit serial-to-parallel converted symbol block in each time slot. The average transmission power is maintained to be unity [11] and the proposed GMP-based receiver is employed at the receivers. Other parameters are all set to the same as previously presented. Consequently, according to (10), the spectral efficiency of STMIM-FTN system, SM system, STSIM system and conventional MIMO system are all 1.11 bps/Hz, except that the STMIM system is 0.97 bps/Hz. As shown in Fig. 3, the STSIM contains inactivated time slots, which leads to not only a waste of resource, but also a serious performance deterioration, as a higher order constellation has to be employed to obtain the same transmission rate. The conventional MIMO system, however, suffers from high ICI over the multipath MIMO channel. The proposed STMIM and STMIM-FTN schemes achieve superior BER performances among the five schemes. Meanwhile, the FTN signaling with $\tau = 0.875$ increases the spectral efficiency of STMIM scheme from 0.97 bps/Hz to 1.11 bps/Hz with only 0.1 dB performance loss. On the other hand, the conventional SM scheme undergoes a 0.6 dB performance loss. Compared with the conventional SM scheme, the STMIM scheme transfers part of the information conveyed by the modulated symbols to the combination pattern of modulation modes, hence it is more robust against interference [1]. In Fig. 4, the parameters $\{N_{\rm TI}, N_{\rm t}; (M_1, \ldots, M_j); \tau\}$ of STMIM-FTN system are set to $\{2, 4; (4, 4); 0.9\}$. The STMIM system with spectral efficiency 1.25 bps/Hz has the system parameter $\{N_{\rm TI}, N_{\rm t}; (M_1, \ldots, M_j)\} = \{2, 4; (4, 4)\}$. The STMIM system with spectral efficiency 1.39 bps/Hz has the system parameter $\{2, 4; (4, 8)\}$, utilizing the $(4, 8)$ constellation alphabet designed in [13] employing Model B. The conventional SM scheme utilizes an 8PSK constellation alphabet. Other parameters are the same as those used in Fig. 3. It can be seen that among systems with spectral efficiency 1.39 bps/Hz, the proposed STMIM-FTN delivers the best performance with performance loss less than 0.3 dB. Although both SM and STMIM increase the spectral efficiency from 1.25 bps/Hz to 1.39 bps/Hz, the combined space-time IM scheme has a better BER performance than its spatial domain IM counterpart resulting from the robustness of IM scheme in time domain.

[2]The number of iterations can also be determined through testing certain stop conditions during the detection. We choose a fixed iteration number here in the simulation to illustrate the convergence behavior of the proposed algorithm.

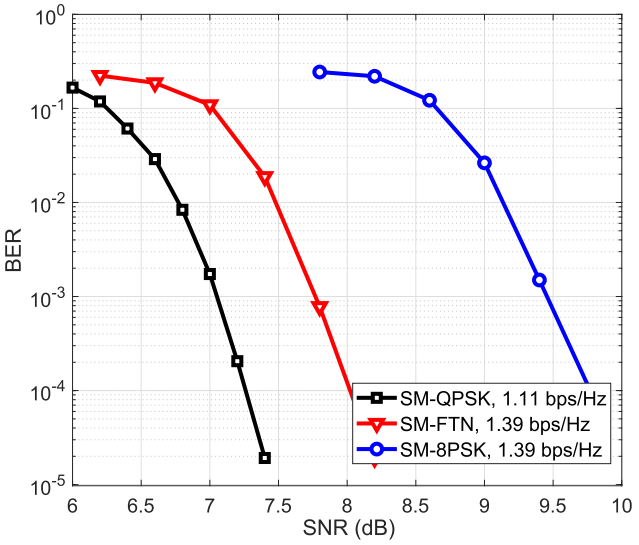

FIGURE 5. BER performance of SM and SM-FTN systems with spectral efficiency 1.11 bps/Hz and 1.39 bps/Hz.

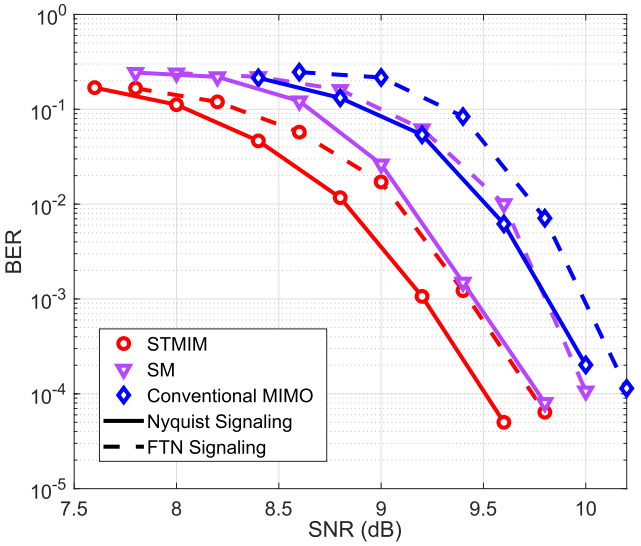

FIGURE 6. BER performance of different systems with and without IM.

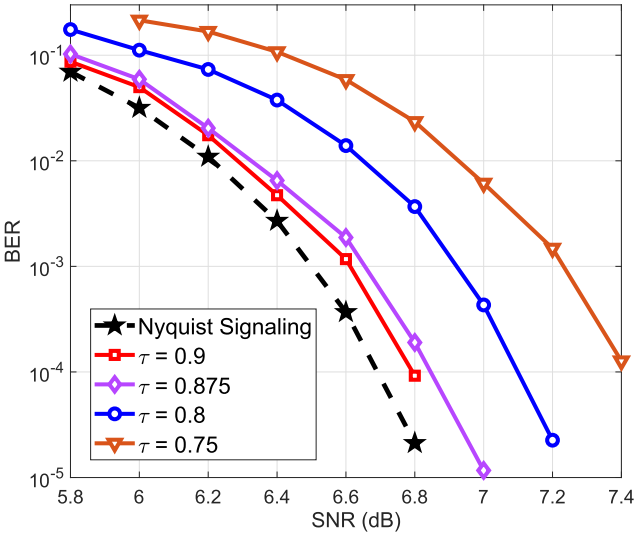

FIGURE 7. BER performance of the proposed GMP-based receiver for STMIM-FTN system with different packing factors.

The BER performance of FTN signaling-aided SM system compared with conventional SM systems is also illustrated in Fig. 5. The SM-QPSK and SM-8PSK employ a QPSK and an 8PSK constellation alphabet, respectively, while the FTN-aided SM system employs a QPSK constellation with the FTN packing ratio $\tau = 0.8$, which increases the spectral efficiency to 1.39 bps/Hz as well. Other parameters are the same as those used in Fig. 4. The SM-8PSK increases the spectral efficiency from 1.11 bps/Hz to 1.39 bps/Hz by conventionally employing higher order constellation, while the SM-FTN utilizes FTN signaling to enhance the spectral efficiency. However, the BER performance loss is more than 2 dB and 0.7 dB, respectively. Consequently, it can be demonstrated that the proposed FTN-aided multi-antenna scheme is able to improve the spectral efficiency with a better BER performance.

Fig. 6 shows the BER performance of the proposed STMIM system, SM system and conventional MIMO system in Nyquist and FTN scenarios. The parameters of SM and STMIM systems are the same as those used in Fig. 5. The conventional MIMO employs a BPSK constellation for a 5×5 MIMO system. The FTN packing ratio is $\tau = 0.9$ for all systems. Hence the spectral efficiency of the three systems in Nyquist and FTN scenarios are all 1.39 bps/Hz and 1.54 bps/Hz, respectively. It can be seen that IM-aided schemes outperform the conventional MIMO scheme in both Nyquist and FTN scenarios. This benefit is achieved because of the robustness of IM schemes in spatial and time domains against interference.

The BER performance of the proposed GMP-based receiver in the STMIM-FTN system with different FTN packing factors is shown in Fig. 7. The system parameters are the same as Fig. 3, unless otherwise stated. Moreover, the performance of Nyquist signaling scenario over the same channel is also plotted as a benchmark. It can be observed that the proposed FTN signaling receiver can approach the BER performance of the Nyquist signaling with a packing factor $\tau \geq 0.875$, i.e. a 14% increase of transmission rate. Even for $\tau = 0.8$, which leads to an increase of transmission rate by more than 25%, the performance gap is around 0.4 dB. However, as for $\tau = 0.75$, which refers to a 33% transmission rate increase, the BER performance exhibits a non-negligible deterioration.

We evaluate the BER performance of STMIM-FTN systems with different roll-off factors β in Fig. 8. Other system parameters are all the same as those used in Fig. 4. It can be shown that the BER performance loss resulting from the pulse smearing effects of FTN signaling becomes greater as β decreases. However, although the performance advantage diminishes as β declines, the proposed FTN-aided system

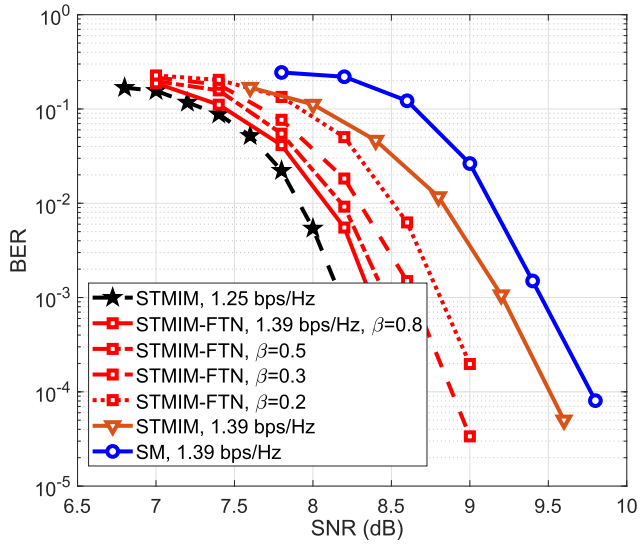

FIGURE 8. BER performance of the proposed STMIM-FTN systems with different β.

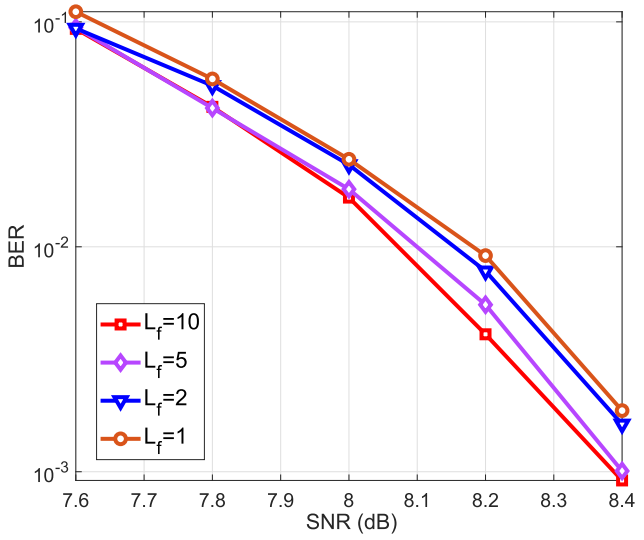

FIGURE 9. BER performance of the proposed GMP-based receiver with different L_f.

still inevitably outperforms its Nyquist signaling counterparts.

BER performances with different L_f are shown in Fig. 9. The parameters $\{N_{\mathrm{TI}}, N_{\mathrm{t}}; (M_1, \ldots, M_j); \tau\}$ are set to $\{2, 4; (4, 4); 0.8\}$. Obviously, the complexity of the proposed FTN equalizer depends on the length of adjacent symbol interference considered at the receiver. As can be seen, the BER gap between different L_f is limited. Specifically, the BER gain owing to the L_f increasing from 5 to 10 is marginal, while $L_f = 2$ and $L_f = 1$ undergoes a performance penalty owing to the underestimation of the ISI length at the receiver. Consequently, the L_f can be properly chosen around 5 in the $\tau = 0.8$ case. In practice, we can select a certain length of L_f properly for the proposed algorithm, considering the tradeoff between the BER performance and the computational complexity.

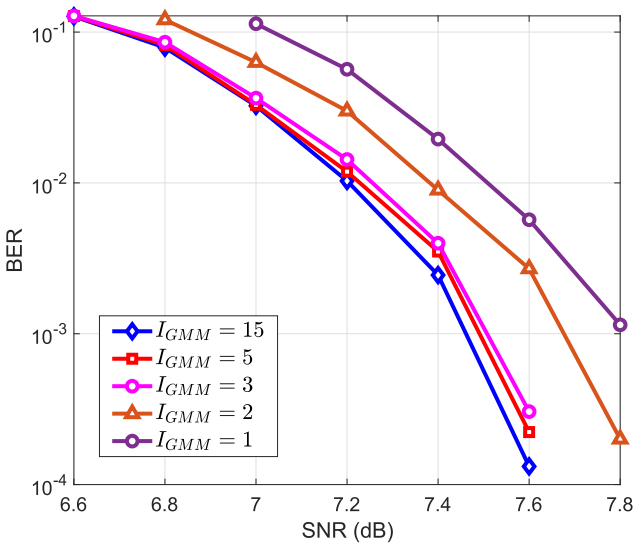

FIGURE 10. Impact of I_{GMM} on BER performance of the proposed GMP-GMM algorithm.

In Fig. 10, the impact of I_{GMM} on the proposed GMP-GMM algorithm is illustrated with $\tau = 0.8$. The I_{GMM} is set to 1, 2, 3, 5, and 15, respectively. The GMP-GMM with $I_{\mathrm{GMM}} = 1$, which leads to a conventional two-step hard decision method, has the worst BER performance among them. As the I_{GMM} increases, i.e. the soft information of IM modes is updated during iterations, the performance of GMP-GMM is improved rapidly. We can see that the BER performance gap between $I_{\mathrm{GMM}} = 5$ and $I_{\mathrm{GMM}} = 15$ is negligible. Even for $I_{\mathrm{GMM}} = 3$, the performance gap is around 0.05 dB.

Furthermore, the convergence behaviors of the iterative message passing algorithms are evaluated in Fig. 11. The convergence of Gaussian belief propagation is not guaranteed in loopy factor graphs [41], while robust convergence can often be observed. In Fig. 11(a), the BER performance of GMP algorithm versus the number of iterations is plotted, with SNR = 6.6 dB, 6.8 dB and 7.2 dB, $\tau = 0.8$, 0.875 and 0.9, respectively. It can be seen that the proposed algorithm has an outstanding convergence performance with all τ. In this scenario, the proposed algorithm converges within 15 iterations. As for the GMP-GMM algorithm with $I_{\mathrm{GMM}} = 3$, the convergence performance is illustrated in Fig. 11(b). In addition, besides its convergence, we can notice that after I_{GMM} iterations, i.e. the candidate set is limited within $\boldsymbol{X}_{l_M}$, the proposed GMP-GMM still achieve gain from iteration, for the modulation mode pattern has been determined through the first I_{GMM} iterations.

We finally compare the BER performance of proposed algorithms for IM scheme, namely IMGMP and IMGMP-GMM respectively, with other methods. Since that there is no existing work that can be applied directly on the proposed STMIM-FTN system, we extend two estimators, namely soft-MMSE extended from [40] and Gaussian-SIC, to the FTN signaling over the same frequency selective

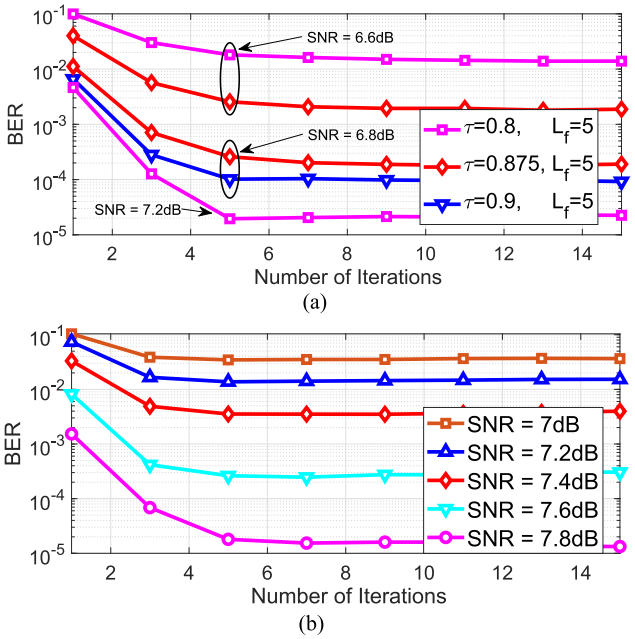

FIGURE 11. BER performance versus number of iterations for the proposed algorithm. (a) GMP. (b) GMP-GMM.

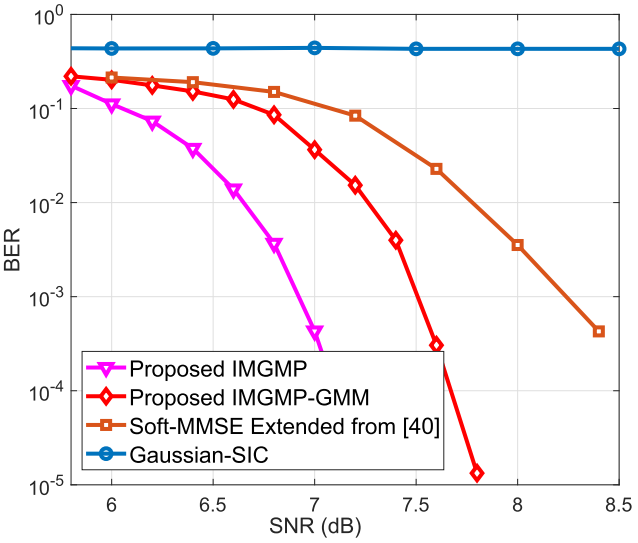

FIGURE 12. BER performance of different algorithms for STMIM-FTN system with parameters {2, 4; (2, 2); 0.8}.

fading MIMO channel. In Fig. 12 and Fig. 13, the parameters $\{N_{\mathrm{TI}}, N_{\mathrm{t}}; (M_1, \ldots, M_j); \tau\}$ are set to $\{2, 4; (2, 2); 0.8\}$ and $\{2, 4; (4, 4); 0.9\}$, respectively. The soft-MMSE equalizer minimize the overall mean square error caused by noise, FTN-induced ISI and fading channel-induced ISI, at the cost of imperfect interference elimination [40]. From Fig. 12, it can be seen that the BER performance gap between the proposed GMP algorithm and GMP-GMM algorithm with $I_{\mathrm{GMM}} = 3$ is less than 0.6 dB. On the other hand, a more than 1.2 dB performance loss can be observed for soft-MMSE method in Fig. 12, whereas an even worse BER

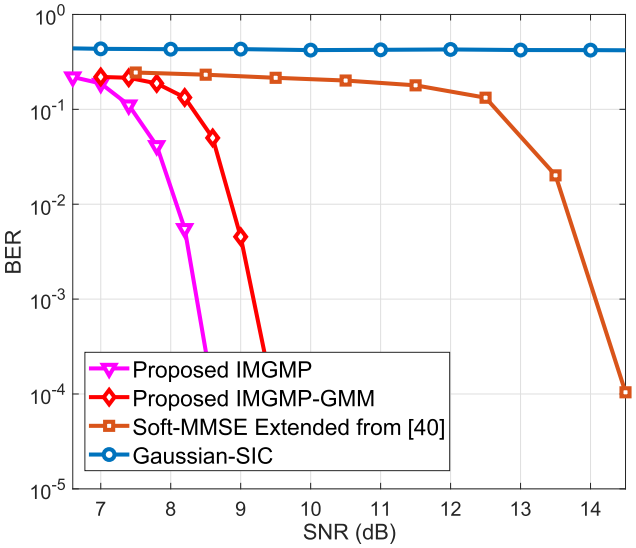

FIGURE 13. BER performance of different algorithms for STMIM-FTN system with parameters {2, 4; (4, 4); 0.9}.

performance can be seen in Fig. 13. The Gaussian-SIC method approximate the noise and ISI interference to be Gaussian. Owing to the straightforward Gaussian approximation, Gaussian-SIC method collapses as the interference becomes severe.

VI. CONCLUSION

In this paper, we proposed an FTN signaling-aided multi-dimensional multi-mode IM scheme, namely STMIM-FTN. Combining multi-mode time-domain IM and SM, the proposed scheme possesses the advantages of SM along with the high efficiency of multi-mode time domain IM. Meanwhile, aided by FTN signaling, the spectral efficiency is further increased with the same bandwidth. At the receiver side, the problem was formulated to a state-space model, leading to a Forney style factor graph. GMP was employed to update the messages on the graph. The ISI imposed by FTN and frequency selective fading channel was mitigated separately, utilizing the truncation of FTN-induced ISI in the proposed algorithm. Moreover, a concise representation of extrinsic messages from the output of equalizer was derived for IM scheme. To further reduce the computational complexity, a two-step LLR calculation was proposed based on GMM. Simulation results showed the superior performance of the proposed STMIM-FTN system compared to other systems with the same spectral efficiency. The outstanding performance of the proposed GMP-based receiver was also evaluated by comparing with other methods.

REFERENCES

[1] T. Mao, Q. Wang, Z. Wang, and S. Chen, "Novel index modulation techniques: A survey," *IEEE Commun. Surveys Tuts.*, vol. 21, no. 1, pp. 315–348, 1st Quart., 2018.

[2] E. Başar, "Index modulation techniques for 5G wireless networks," *IEEE Commun. Mag.*, vol. 54, no. 7, pp. 168–175, Jul. 2016.

[3] S. Sugiura, T. Ishihara, and M. Nakao, "State-of-the-art design of index modulation in the space, time, and frequency domains: Benefits and fundamental limitations," *IEEE Access*, vol. 5, pp. 21774–21790, 2017.

[4] P. Yang, M. Di Renzo, Y. Xiao, S. Li, and L. Hanzo, "Design guidelines for spatial modulation," *IEEE Commun. Surveys Tuts.*, vol. 17, no. 1, pp. 6–26, 1st Quart., 2015.

[5] J. Wang, S. Jia, and J. Song, "Generalised spatial modulation system with multiple active transmit antennas and low complexity detection scheme," *IEEE Trans. Wireless Commun.*, vol. 11, no. 4, pp. 1605–1615, Apr. 2012.

[6] S. Sugiura and L. Hanzo, "Single-RF spatial modulation requires single-carrier transmission: Frequency-domain turbo equalization for dispersive channels," *IEEE Trans. Veh. Technol.*, vol. 64, no. 10, pp. 4870–4875, Oct. 2015.

[7] R. Abu-Alhiga and H. Haas, "Subcarrier-index modulation OFDM," in *Proc. IEEE Int. Symp. Pers., Indoor, Mobile Radio Commun.*, Sep. 2009, pp. 177–181.

[8] N. Ishikawa, S. Sugiura, and L. Hanzo, "Subcarrier-index modulation aided OFDM—will it work?" *IEEE Access*, vol. 4, pp. 2580–2593, 2016.

[9] Y. Cai, Z. Qin, F. Cui, G. Y. Li, and J. A. McCann, "Modulation and multiple access for 5G networks," *IEEE Commun. Surveys Tuts.*, vol. 20, no. 1, pp. 629–646, 1st Quart., 2018.

[10] M. Nakao, T. Ishihara, and S. Sugiura, "Single-carrier frequency-domain equalization with index modulation," *IEEE Commun. Lett.*, vol. 21, no. 2, pp. 298–301, Feb. 2017.

[11] T. Ishihara and S. Sugiura, "Faster-than-Nyquist signaling with index modulation," *IEEE Wireless Commun. Lett.*, vol. 6, no. 5, pp. 630–633, Oct. 2017.

[12] T. Mao, Z. Wang, Q. Wang, S. Chen, and L. Hanzo, "Dual-mode index modulation aided OFDM," *IEEE Access*, vol. 5, pp. 50–60, 2017.

[13] M. Nakao, T. Ishihara, and S. Sugiura, "Dual-mode time-domain index modulation for Nyquist-criterion and faster-than-Nyquist single-carrier transmissions," *IEEE Access*, vol. 5, pp. 27659–27667, 2017.

[14] M. Wen, E. Basar, Q. Li, B. Zheng, and M. Zhang, "Multiple-mode orthogonal frequency division multiplexing with index modulation," *IEEE Trans. Commun.*, vol. 65, no. 9, pp. 3892–3906, Sep. 2017.

[15] J. Li, M. Wen, X. Jiang, and W. Duan, "Space-time multiple-mode orthogonal frequency division multiplexing with index modulation," *IEEE Access*, vol. 5, pp. 23212–23222, 2017.

[16] M. Wen, Q. Li, E. Basar, and W. Zhang, "Generalized multiple-mode OFDM with index modulation," *IEEE Trans. Wireless Commun.*, vol. 17, no. 10, pp. 6531–6543, Oct. 2018.

[17] Q. Li, M. Wen, E. Basar, H. V. Poor, B. Zheng, and F. Chen, "Diversity enhancing multiple-mode OFDM with index modulation," *IEEE Trans. Commun.*, vol. 66, no. 8, pp. 3653–3666, Aug. 2018.

[18] S. Sugiura, S. Chen, and L. Hanzo, "Coherent and differential space-time shift keying: A dispersion matrix approach," *IEEE Trans. Commun.*, vol. 58, no. 11, pp. 3219–3230, Nov. 2010.

[19] S. Sugiura, S. Chen, and L. Hanzo, "Generalized space-time shift keying designed for flexible diversity-, multiplexing- and complexity-tradeoffs," *IEEE Trans. Wireless Commun.*, vol. 10, no. 4, pp. 1144–1153, Apr. 2011.

[20] B. Shamasundar, S. Bhat, S. Jacob, and A. Chockalingam, "Multidimensional index modulation in wireless communications," *IEEE Access*, vol. 6, pp. 589–604, 2017.

[21] S. Jacob, T. L. Narasimhan, and A. Chockalingam, "Space-time index modulation," in *Proc. IEEE Wireless Commun. Netw. Conf. (WCNC)*, Mar. 2017, pp. 1–6.

[22] T. Mao, Q. Wang, and Z. Wang, "Generalized dual-mode index modulation aided OFDM," *IEEE Commun. Lett.*, vol. 21, no. 4, pp. 761–764, Apr. 2017.

[23] L. Xiao, Y. Xiao, Y. Zhao, P. Yang, M. Di Renzo, S. Li, and W. Xiang, "Time-domain turbo equalization for single-carrier generalized spatial modulation," *IEEE Trans. Wireless Commun.*, vol. 16, no. 9, pp. 5702–5716, Sep. 2017.

[24] M. Tuchler, A. C. Singer, and R. Koetter, "Minimum mean squared error equalization using a priori information," *IEEE Trans. Signal Process.*, vol. 50, no. 3, pp. 673–683, Mar. 2002.

[25] X. Wang and H. V. Poor, "Iterative (turbo) soft interference cancellation and decoding for coded CDMA," *IEEE Trans. Commun.*, vol. 47, no. 7, pp. 1046–1061, Jul. 1999.

[26] T. Abe and T. Matsumoto, "Space-time turbo equalization in frequency-selective MIMO channels," *IEEE Trans. Veh. Technol.*, vol. 52, no. 3, pp. 469–475, May 2003.

[27] Y. Zhao, P. Yang, Y. Xiao, L. Xiao, B. Dong, and W. Xiang, "An improved frequency domain turbo equalizer for single-carrier spatial modulation systems," *IEEE Trans. Veh. Technol.*, vol. 66, no. 8, pp. 7568–7572, Aug. 2017.

[28] J. E. Mazo, "Faster-than-Nyquist signaling," *Bell Syst. Tech. J.*, vol. 54, no. 8, pp. 1451–1462, 1975.

[29] J. B. Anderson, F. Rusek, and V. Öwall, "Faster-than-Nyquist signaling," *Proc. IEEE*, vol. 101, no. 8, pp. 1817–1830, Aug. 2013.

[30] F. Rusek and J. B. Anderson, "The two dimensional Mazo limit," in *Proc. IEEE Int. Symp. Inf. Theory*, Sep. 2005, pp. 970–974.

[31] H.-A. Loeliger, "An introduction to factor graphs," *IEEE Signal Process. Mag.*, vol. 21, no. 1, pp. 28–41, Jan. 2004.

[32] W. Yuan, N. Wu, Q. Guo, Y. Li, C. Xing, and J. Kuang, "Iterative receivers for downlink MIMO-SCMA: Message passing and distributed cooperative detection," *IEEE Trans. Wireless Commun.*, vol. 17, no. 5, pp. 3444–3458, May 2018.

[33] S. Wu, L. Kuang, Z. Ni, J. Lu, D. Huang, and Q. Guo, "Low-complexity iterative detection for large-scale multiuser MIMO-OFDM systems using approximate message passing," *IEEE J. Sel. Topics Signal Process.*, vol. 8, no. 5, pp. 902–915, May 2014.

[34] Q. Shi, N. Wu, X. Ma, and H. Wang, "Frequency-domain joint channel estimation and decoding for faster-than-Nyquist signaling," *IEEE Trans. Commun.*, vol. 66, no. 2, pp. 781–795, Feb. 2018.

[35] S. Sugiura and L. Hanzo, "Frequency-domain-equalization-aided iterative detection of faster-than-Nyquist signaling," *IEEE Trans. Veh. Technol.*, vol. 64, no. 5, pp. 2122–2128, May 2015.

[36] N. Wu, W. Yuan, H. Wang, Q. Shi, and J. Kuang, "Frequency-domain iterative message passing receiver for faster-than-Nyquist signaling in doubly selective channels," *IEEE Wireless Commun. Lett.*, vol. 5, no. 6, pp. 584–587, Dec. 2016.

[37] N. Wu, W. Yuan, Q. Guo, and J. Kuang, "A hybrid BP-EP-VMP approach to joint channel estimation and decoding for FTN signaling over frequency selective fading channels," *IEEE Access*, vol. 5, pp. 6849–6858, May 2017.

[38] H.-A. Loeliger, J. Dauwels, J. Hu, S. Korl, L. Ping, and F. R. Kschischang, "The factor graph approach to model-based signal processing," *Proc. IEEE*, vol. 95, no. 6, pp. 1295–1322, Jun. 2007.

[39] Q. Guo and D. D. Huang, "A concise representation for the soft-in soft-out LMMSE detector," *IEEE Commun. Lett.*, vol. 15, no. 5, pp. 566–568, May 2011.

[40] P. Shang, S. Kim, and K. Choi, "Soft MMSE receiver for turbo coded MIMO system," in *Proc. IEEE 7th Int. Conf. Wireless Mobile Comput., Netw. Commun.*, Oct. 2011, pp. 471–475.

[41] B. Li and Y.-C. Wu, "Convergence analysis of Gaussian belief propagation under high-order factorization and asynchronous scheduling," *IEEE Trans. Signal Process.*, vol. 67, no. 11, pp. 2884–2897, Jun. 2019.

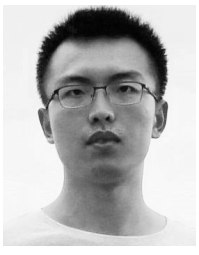

SHAOANG LI received the B.S. degree in communication engineering from Northwestern Polytechnical University, Xi'an, China, in 2017. He is currently pursuing the master's degree with the School of Information and Electronics, Beijing Institute of Technology, Beijing, China. His research interests include statistical inference on graphical models and wireless communications.

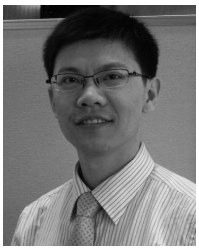

NAN WU (M'11) received the B.S., M.S., and Ph.D. degrees from the Beijing Institute of Technology (BIT), Beijing, China, in 2003, 2005, and 2011, respectively. From 2008 to 2009, he was a Visiting Ph.D. Student with the Department of Electrical Engineering, Pennsylvania State University, USA. He is currently a Professor with the School of Information and Electronics, BIT. His research interests include signal processing in wireless communication networks. He was a recipient of the National Excellent Doctoral Dissertation Award by MOE of China, in 2013. He serves as an Associate Editor for IEEE Access, the *International Journal of Electronics and Communications*, the *KSII Transactions on Internet and Information Systems*, and the *IEICE Transactions on Communications*.

QIAOLIN SHI (S'15) received the B.S. degree from the Beijing Institute of Technology, Beijing, China, in 2014, where she is currently pursuing the Ph.D. degree with the School of Information and Electronics. Her research interest includes statistical learning on graphical models and its application to wireless communications. She has served as a Reviewer for several international journals and conferences.

QINGHUA GUO (S'07–M'08–SM'18) received the B.E. degree in electronic engineering and the M.E. degree in signal and information processing from Xidian University, Xi'an, China, in 2001 and 2004, respectively, and the Ph.D. degree in electronic engineering from the City University of Hong Kong, Hong Kong, in 2008. He is currently an Associate Professor with the School of Electrical, Computer and Telecommunications Engineering, University of Wollongong, Wollongong, NSW, Australia, and an Adjunct Associate Professor with the School of Engineering, The University of Western Australia, Perth, WA, Australia. His research interests include signal processing and telecommunications. He was a recipient of the Australian Research Council's Inaugural Discovery Early Career Researcher Award, in 2012.